fermentation

MDPI

Article

Single-Cell Optical Nanomotion of *Candida albicans* in Microwells for Rapid Antifungal Susceptibility Testing

Vjera Radonicic [1,2,3], Charlotte Yvanoff [1,2,3], Maria Ines Villalba [3,4], Bart Devreese [2,5], Sandor Kasas [3,4,6,†] and Ronnie G. Willaert [1,2,3,*,†]

1 Research Group Structural Biology Brussels, Vrije Universiteit Brussel, 1050 Brussels, Belgium
2 Alliance Research Group VUB-UGent NanoMicrobiology (NAMI), Vrije Universiteit Brussel, 1050 Brussels, Belgium
3 International Joint Research Group VUB-EPFL NanoBiotechnology & NanoMedicine (NANO), Vrije Universiteit Brussel, 1050 Brussels, Belgium
4 Laboratory of Biological Electron Microscopy, Ecole Polytechnique Fédérale de Lausanne (EPFL), University of Lausanne, 1015 Lausanne, Switzerland
5 Laboratory of Microbiology, Department of Biochemistry and Microbiology, Ghent University, 9000 Ghent, Belgium
6 Centre Universitaire Romand de Médecine Légale, UFAM, Université de Lausanne, 1015 Lausanne, Switzerland
* Correspondence: ronnie.willaert@vub.be; Tel.: +32-2-6291846
† These authors contributed equally to this work.

Abstract: *Candida albicans* is an emerging multidrug-resistant opportunistic pathogen representing an important source of invasive disease in humans and generating high healthcare costs worldwide. The development of a rapid and simple antifungal susceptibility test (AFST) could limit the spread of this disease, increase the efficiency of treatment, and lower the risk of developing resistant strains. We developed a microfluidic chip containing an array of microwells that were designed to trap the cells and perform rapid antifungal susceptibility tests using optical nanomotion detection (ONMD). Yeast cell entrapment in a microwell allows for a very rapid exchange of growth medium with the antifungal, which enables performing single-cell ONMD measurements on the same cell before and after antifungal treatment. The exposure to a low concentration of the antifungal caspofungin or flucanozole induced a significant decrease in the nanomotion signal, demonstrating the high sensitivity of this technique. We used this chip to quantify the real-time response of individual *C. albicans* cells to the antifungal treatment in as fast as 10 min. This simple and label-free technique could be further developed into a simple-to-use device that allows the performance of fast AFST as part of a routine hospital procedure in developed and also eventually developing world countries.

Keywords: cellular nanomotion; single cell; optical nanomotion detection; microfluidic chip; microwells; yeast; *Candida albicans*; antifungal; antifungal susceptibility testing

Citation: Radonicic, V.; Yvanoff, C.; Villalba, M.I.; Devreese, B.; Kasas, S.; Willaert, R.G. Single-Cell Optical Nanomotion of *Candida albicans* in Microwells for Rapid Antifungal Susceptibility Testing. *Fermentation* **2023**, *9*, 365. https://doi.org/10.3390/fermentation9040365

Academic Editor: Alexander Rapoport

Received: 13 February 2023
Revised: 1 April 2023
Accepted: 2 April 2023
Published: 7 April 2023

1. Introduction

Most human fungal infections are caused by the species that belong to the genus *Candida*. The most frequent species that cause opportunistic infections include *C. albicans*, *C. glabrata*, *C. auris*, *C. tropicalis*, *C. parapsilosis*, and *C. krusei* [1]. *C. albicans* are frequently found as an important part of the microbial flora of healthy persons and can induce systemic and superficial infections under certain environmental conditions [2]. This species causes a variety of diseases that range from vaginal infections, which affect up to 75% of women at least once in their lifetime [3], to oral infections and may also, under favourable conditions, enter the bloodstream leading to deep-tissue infections [2]. *C. albicans* may also play a role in the persistence or worsening of some chronic inflammatory bowel diseases [3]. Furthermore, invasive candidiasis (IC) is an important nosocomial infection with high morbidity and mortality rates in hospitalised children (oncology patients) [4]. Finally,

Candida species present a major source of extended infections in intensive care patients (ICU), especially in patients who are immunocompromised or elderly [2]

The fast emergence of multi-resistant pathogenic *Candida* species is caused by the extensive and sometimes unnecessary use of broad-spectrum antifungals [2]. Hence, the development of rapid antifungal sensitivity tests could allow for the identification and use of more selective antifungals, thereby reducing the spread of pathogenic fungi and their evolution toward a multi-resistant phenotype [5–7]. A "rapid" AST is usually defined as a test that can be performed within a single working shift, i.e., within 8 h or less [8].

Standard methods to perform AFST rely on measuring fungal growth in the presence of antifungals over a long period (usually a few days) [9]. Traditional antimicrobial susceptibility testing (AST) methods include disc diffusion and broth dilution assays, which rely on the observation of the growth of microorganisms in the presence of specific antimicrobials under defined test conditions. Commercially available tests, such as Sensititre YeastOne, Etest, and the fully automated VITEK2 (bioMérieux), MicroScan WalkAway (Siemens Healthcare Diagnostics), BD Phoenix (BD Diagnostics) and Sensititre ARIS 2X (Trek Diagnostic Systems), are also widely used to test antifungal susceptibility [8,10]. Some of these tests require a long period of analysis time. VITEK2 (bioMérieux), MicroScan WalkAway (Siemens Healthcare Diagnostics) and BD Phoenix (BD Diagnostics) can generate rapid results (3.5–16 h). However, it must be noted that they require a standardised microbial inoculum (24–48 h or more) prior to their inoculation into the AST system [8].

More rapidly emerging AST methods with different approaches have been reported, including the use of laser scatter technology [11], the sensing of bacterial vibrations using phase-noise measurements on resonant piezo-electric substrates [12], protein-adsorbed magnetic nanoparticle-mediated protocols [13], field-effect enzymatic detection [14], glucose metabolisation [15], optical screening and diffusometry [16], nanometre-scale bacterial deformation measurement [17], mass spectrometry [18], nanowire sensors [19], electrochemical sensing [20], real-time laser scattering [21], fluorescence-activated cell sorting (FACS) [22], Raman and infrared spectroscopy at the single-cell level [23–25] nanotube-assisted microwave electroporation [24], hydrodynamic trapping [26] and phenotypic AST [27]. New and more advanced diagnostic methods use matrix-assisted laser desorption ionisation time-of-flight mass spectroscopy (MALDI-TOF-MS). Very recently, a microdroplet-based MALDI-TOF-MS approach for the performance of rapid AST was presented [28], which required an incubation period of 3 or 4 h for the data acquisition. However, clinical trials have still not demonstrated the direct detection of resistance factors [29].

Over the last few years, atomic force microscope (AFM)-based sensitivity tests have been developed to assess the sensitivity of microorganisms to a given drug in a timeframe of minutes [30,31]. This method consists of attaching the cells to an AFM cantilever, treating them with an antimicrobial drug, and monitoring their oscillations (referred to as "cellular nanomotion" since the displacements of the cantilever are of the nanometer order) as a function of time. Numerous studies demonstrated that living organisms attached to AFM cantilevers induce oscillations of the lever that immediately stop when the organisms die [32,33]. Cellular nanomotion detection (NMD) proved the detection of living organisms in a chemistry-independent manner and in a very time-efficient way [34,35]. Nevertheless, this method has some drawbacks. AFMs are expensive and relatively complex devices that require expertise to operate. Additionally, such nanomotion detectors are relatively complex to scale up and can only monitor one bacterial/fungal species at a time. Finally, it is not a single-cell method.

Other fast AST methods have also been developed to detect the nanomotion of living microorganisms that are attached to a surface. These include the plasmonic imaging of the z motion of attached bacteria [36], the sensing of attached bacterial vibrations with the phase noise of a resonant crystal [12], tracking the x-y motion of attached uropathogenic *Escherichia coli* [37], and subcellular fluctuation imaging, which is based on total internal

reflection microscopy (TIRM) [38], as well as optically tracking bacterial responses on micropillar architectures using intrinsic phase-shift spectroscopy [39].

Recently, we found that a simple optical microscope equipped with a video camera can also detect living cells' nanometric scale oscillations at a subpixel resolution using dedicated software [40]. We applied this "optical nanomotion detection" (ONMD) method to assess the susceptibility of various yeasts to antifungals. Previously, we developed a microfluidic chip with a "no-flow" chamber that allowed the exchange of a growth medium with antimicrobial agents without disturbing the nanomotion of the cells [41]. The no-flow chamber allowed us to observe the nanomotion of a single cell before, during, and after treatment with an antifungal. This measurement was relatively fast, simple, and inexpensive.

Here, we further improved this technique by designing a microwell-based chip and testing its efficiency. The new device traps single cells in microwells and permits the observation of their nanomotion before, during, and after treatment with a chemical compound. The opportunistic yeast *C. albicans* was used to evaluate the device and the effect of caspofungin on individual yeast cells, which were successfully assessed by monitoring their nanomotion pattern as a function of time. We successfully explored the effects of caspofungin on wild-type CAF2-1, fluconazole, and caspofungin on azole-hypersensitive DSY1024 yeast strains and showed that the susceptibility of the cells to caspofungin and fluconazole could be assessed within 10 min. We are convinced that the simplicity and cost efficiency of this new technique will open novel avenues in the field of rapid AFST.

2. Materials and Methods

2.1. Yeast Cultivation

For the selection of the microwell size and shape, we used *Saccharomyces cerevisiae* BY4742 (genotype: *MATα his3Δ1 leu2Δ0 lys2Δ0 ura3Δ0*). Yeast cells were cultured by the overnight inoculation of 20 mL YPD medium (10 g/L yeast extract, 20 g/L peptone, 20 g/L dextrose) with a colony from a YPD agar (YPD containing 20 g/L agar) plate in 100 mL Erlenmeyer flasks with ridges for better aeration at 30 °C and 180 revolutions per minute (rpm) (Innova 4400, New Brunswick, Edison, NJ, USA). The overnight cultures were diluted in a YPD medium to obtain an optical density at 600 nm ($OD_{600\,nm}$) of 0.5 and were then grown in Erlenmeyer flasks for 1 h at 30 °C and 180 rpm. The cultures were further diluted, depending on the cell concentration ($OD_{600\,nm}$ value), to obtain an optimal number of cells and allow for single-cell visualisation in each imaging microwell.

For the antifungal susceptibility testing experiments, we used *C. albicans* strains CAF2-1 (genotype: Δ*ura3::imm434/URA3*) [42,43] and DSY1024 (mutant for efflux systems; genotype: Δ*cdr1:hisG/*Δ*cdr1::hisG;* Δ*cdr2::hisG;* Δ*flu1::hisG/*Δ*flu1::hisG;* Δ*mdr1::hisG-URA3-hisG/*Δ*mdr1::hisG*) [42]. The yeast cells were cultured by inoculating 20 mL of a YPD medium with a colony from a YPD agar plate. The cultures were grown overnight in 100 mL Erlenmeyer flasks with ridges for better aeration at 30 °C and 180 revolutions per minute (rpm). The overnight cultures were diluted in a YPD medium to obtain an optical density at 600 nm ($OD_{600\,nm}$) of 0.1 and were then grown in Erlenmeyer flasks for 1 h at 30 °C and 180 rpm. The cultures were further diluted to obtain an optical density at 600 nm ($OD_{600\,nm}$) of 0.03. This allowed us to obtain single cells per well.

2.2. Microfluidic Chip Construction

The microwell layer of the microfluidic chip was fabricated using soft lithography. The design of the microfluidic chip (20 × 87 microwells) was made in DesignSpark Mechanical (www.rs-online.com, 1 May 2022) and then transferred onto a film photomask (0.18 mm polyester with photo emulsion layer) using a laser-photoplotter (Selba S.A., Versoix, Switzerland). The mould for the microwell layer was created using photolithography onto a silicon wafer (4-inch Test CZ-Si wafer, Microchemicals GmbH, Ulm, Germany). The wafer was cleaned in acetone (Carl Roth, Karlsruhe, Germany) and 2-propanol (Carl Roth,

Karlsruhe, Germany) for 5 min each before being rinsed with ultrapure water and, finally, air blow-dried. The wafer was then heated on a hot plate (Torrey Pines Scientific, Carlsbad, CA, USA) at 100 °C to ensure that all the residual solvents were evaporated. The wafer was then exposed to air plasma at 100 W, 50 kHz, for 1 min (Plasma System Cute, Femto Science, Dongtangiheung-Ro, Korea) to ensure more uniformed spin-coating. The mould was fabricated by spin-coating the negative photoresist layer SU-8 3050 (Kayaku Advanced Materials, Westborough, MA, USA) onto the wafer at 3500 rpm for 30 s, which was then soft-baked for 15 min at 95 °C on a hot plate, to reach an approximative thickness of 56 µm. The wafer and the wells' photomask were brought into hard contact in the mask aligner UV-KUB3 (Kloé, Saint-Mathieu-de-Tréviers, France) and was illuminated at 365 nm ultraviolet (UV) light (intensity of 35 mW/cm^2) for 12 s. Next, the wafer was post-baked for 5 min at 95 °C on a hot plate. Finally, the wafer was immersed in a SU-8 developer (Kayaku Advanced Materials, Westborough, MA, USA) for 6 min and then washed with 2-propanol and blow-dried. The dimensions of the wells were measured with a 3-D profilometer (Profilm 3 D, Filmetrics, San Diego, CA, USA).

The SU-8 mould was cleaned from (in-)organic residue by rinsing it with acetone, 2-propanol, and ultrapure water and blow-dried with air. The mould was then exposed to air plasma at 100 W, 50 kHz, for 5 min (Plasma System Cute, Femto Science, Dongtangiheung-Ro, Korea). Next, a sacrificial photoresist layer AZ 1514 H (MicroChemicals GmbH, Ulm, Germany) was spun-coated onto the mould at 4000 rpm for 2 min to obtain a thickness of approximately 3 µm before being soft-baked for 2 min at 100 °C. The polydimethylsiloxane (PDMS) (Sylgard 184 Silicone Elastomer Kit, Dow Inc., Midland, MI, USA) was prepared by mixing the base and the curing agent at a 10:1 ratio which was then degassed in a glass bell for 20 min. Afterward, the PDMS was poured onto the mould and covered with a coverslip glass (25 × 75 mm, 170 µm thickness) and pressed to obtain a thin layer of PDMS (membrane) (Figure 1). By pressing the coverslip glass, air bubbles were introduced, and the chip was degassed again in the glass bell. Afterward, the PDMS was cured for 10 min at 100 °C on a hot plate. The excess PDMS around the coverslip glass was cut off and the mould was submerged in acetone. The acetone dissolved the sacrificial photoresist layer, and the PDMS membrane with wells attached to the coverslip glass, which was easily removed from the mould. Finally, the microfluidic chip was assembled by aligning and sticking the coverslip glass with the PDMS microwells a sticky µ-Slide VI 0.4 channel slides with a double-sided sticky tape of 130 µm thickness (Ibidi GmbH, Gräfelfing, Germany) making six different channels with microwells (Figure 1).

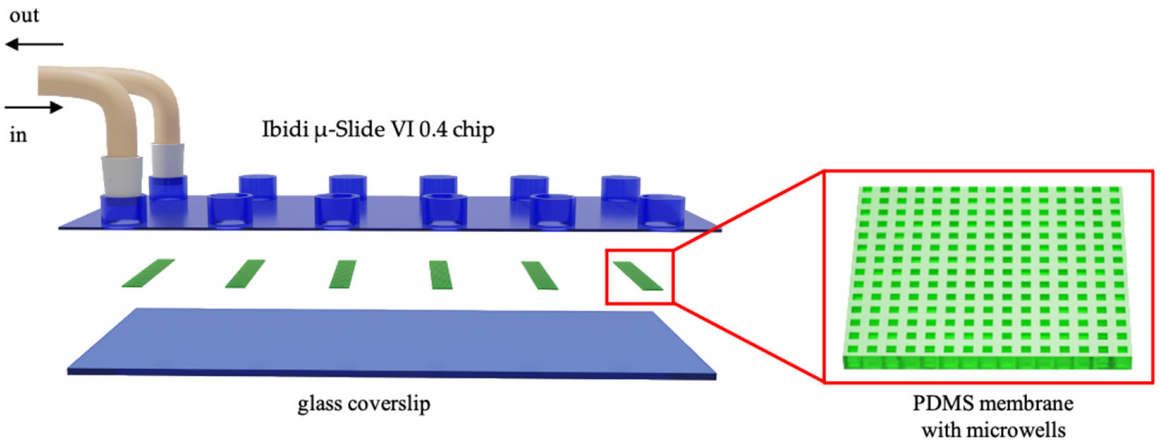

Figure 1. Assembly of the microfluidic chip for cellular nanomotion measurement. The bottom of the chip is composed of 6 PDMS membranes attached to a glass coverslip in such a way that they are aligned with the 6 channels of a sticky Ibidi µ-Slide VI 0.4 chip, used as the top plate. Each PDMS membrane consists of a 20 × 87 array of microwells.

2.3. Computational Simulation of Fluid Flow in the Microfluidic Chip

To simulate the fluid flow in the designed microwells in the channel, fluid flow simulations were performed in 3D using COMSOL Multiphysics 6.1 (COMSOL, Stockholm, Sweden) and by selecting "fluid flow" (single-phase flow, laminar flow) physics. Water at 20 °C was selected as the working liquid. A laminar fluid flow through the channels was simulated with laminar inflow as a boundary condition at the inlet. The inlet flow rate was set at 120 µL/min, which corresponds to the inlet flow rate that was used during the actual experiments. Pressure (atmospheric pressure) was selected as the boundary condition at the outlet, and backflow was suppressed. The physics-controlled mesh was selected as the mesh settings with a normal element size. Particle tracing for the fluid flow physics module of COMSOL was used to calculate the motion of the particles in a background laminar fluid flow in the channel and the microwell. A hundred particles were released at the inlet, with a diameter of 4 µm which corresponded to the size of a yeast cell, and 1 cell was positioned in the microwell. The density of the particles was set at 1117 kg/m^3, which is the average value for yeast cells found in the literature [44–47].

2.4. Microfluidic Chip Setup

The inlet and outlet of the imaging chambers were connected to a pressure-driven pump (LineUp™ Push-Pull, Fluigent, Le Kremlin-Bicêtre, France) via fluorinated ethylene propylene (FEP) tubing with an internal diameter of 0.51 mm. The microfluidic chip setup was then mounted onto an inverted Nikon Eclipse Ti2 epifluorescence microscope (Nikon, Tokyo, Japan) to perform ONMD with bright-field microscopy. The microfluidic chip and tubing were first flushed with ethanol 70% (*v*/*v*) to sterilize them and remove any air bubbles. Then, the tubing and the chip were flushed with a YPD medium to remove any residual ethanol. Next, the yeast liquid culture in YPD was filled into the channels at a flow rate of 120 µL/min and used the pressure-driven pump for 5 min. Then, the pressure pump was turned off to allow the cells to sediment in the wells. Afterward, the YPD medium was flushed through again to clear out any surplus cells. The first ONMD movie was acquired and labeled as "0 min". The solution containing the antifungal caspofungin (Sigma-Aldrich, Overijse, Belgium) or fluconazole (Sigma-Aldrich, Overijse, Belgium) was then filled in from the inlet at a flow rate of 120 µL/min, using the pressure-driven pump for 10 min (until all the liquid in the channel was exchanged with the treatment). Approximately 5 min after turning off the pumps, the second movie was acquired, which corresponded to 10 min after treatment. Each subsequent movie was taken at 1 h time intervals for 5 h. This estimate was based on the time required to pump the compound through the tubing with a flow rate of 120 µL/min and the time it took for the compound to reach a maximal concentration at the bottom of the well.

To observe how the channels and wells were filled, we used the fluorescent dye propidium iodide (PI, Sigma-Aldrich, Overijse, Belgium). The chip was filled with the dye at a flow rate of 120 µL/min (the flow rate used for filling in the antifungal) and 10 µL/min. The movie was acquired at a frame rate of 1 fps (frame/second), at the magnification of 60×, and was later analysed in Fiji ImageJ. We analysed the brightness intensity of the dye in two planes: at the bottom of the well and in the channel and 200 µm above the well (area 100 × 100 px).

2.5. Nanomotion Measurement and Analysis

Cellular nanomotion was monitored by recording bright-field movies of 300 frames at a framerate of 21 fps with an EMCCD camera (Andor) using a 40× objective (1 pixel corresponded to 0.2 µm). The movies were analysed using the cross-correlation analysis method [48] described previously [40]. The ONMD algorithm (MATLAB, MathWorks) works by calculating the x-y displacement of individual cells for each frame. The trajectories of the tracked cells and the root mean square of the displacement are then saved to an MS Excel file. The distribution of the displacements per frame was represented as violin and box-and-whisker (10th to 90th percentile) plots, whereas the total displacements for all cells

were represented as box-and-whisker plots (Prism8, GraphPad). The changes in pixels from frame to frame (differential image) could also be calculated and presented utilizing the software and using a colour scale: the pixels that changed the most were indicated in red, whereas the ones that changed the least were shown in blue (in house MATLAB program).

2.6. Cell Nanomotion and Viability Evaluation

To perform a viability test wild type, strain *C. albicans* CAF2-1 was used. The microfluidic chip with microwells was first sterilized with 70% ethanol and then rinsed with a YPD growth medium, and the microwells in the chip were filled with cells (as described in 2.4). The first set of videos was made and designated as time zero. Next, the chip was filled with propidium iodide (PI) solution (final concentration 5 µg/mL dissolved in water), which was left to incubate for 15 min to stain dead cells [49]. After a set of pictures were made, the liquid in the microfluidic chip was exchanged with 70% (v/v) ethanol, and the cells were treated for 1 h. A new set of videos was acquired to determine the nanomotion signal of dead cells. Next, the cells were once again stained with PI by exchanging the liquid in the chip, and the viability of the cells was determined.

3. Results

3.1. Construction of the Microfluidic Chip

Using soft lithography, we constructed the mould used for the fabrication of the PDMS membrane containing microwells. Using 3-D profilometer imaging, it was shown that the dimensions of the pillars on the mould (Figure 2A) (corresponding to the microwells in the PDMS membrane (Figure 2C, zoom)) matched the design specifications. The PDMS membrane was deposited onto a glass slide, and a sticky Ibidi µ-Slide VI 0.4 was used as a top plate (Figure 2B,C). This resulted in a sealed microfluidic chip with 6 channels with wells (Figure 2C).

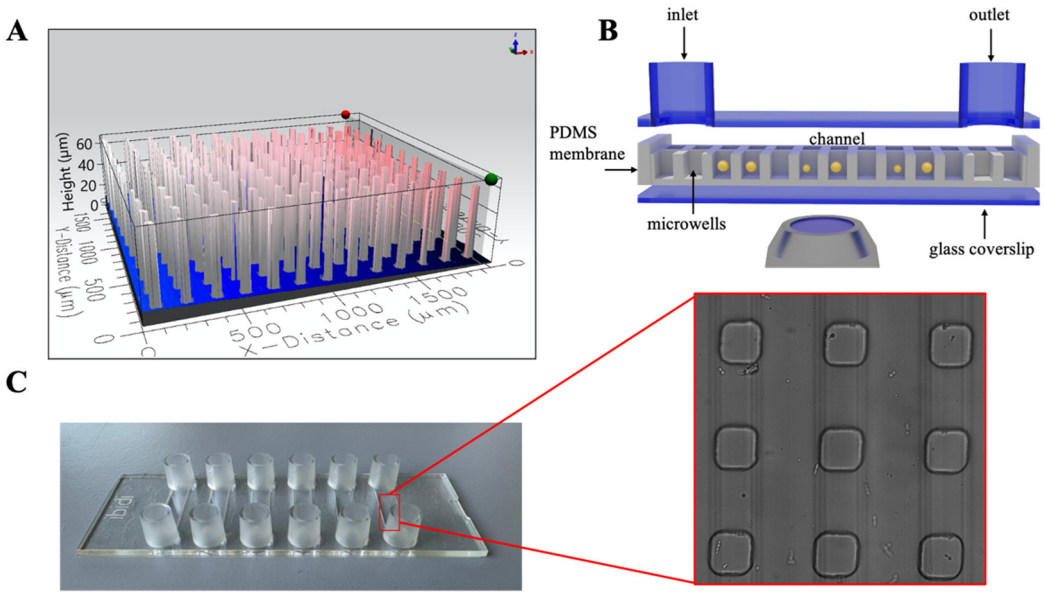

Figure 2. (**A**) Dimensions of a 3D model of the SU8 mould with pillars (3-D profilometer). (**B**) Schematic cross-section of the assembled microfluidic chip filled with yeast cells (yellow dots) (**C**) Picture of the complete microfluidic chip and bright-field image of the microwells filled with cells.

3.1.1. Selection of the Microwell Shape and Dimensions

To assess the optimal size of the microwells, we observed the nanomotion of single *S. cerevisiae* cells in wells of different sizes and shapes. Firstly, we evaluated the influence of the diameter of cylindrical microwells on yeast nanomotion patterns. We tested commercially available cylindrical microwells (MWA-015-08-02, Microsurfaces, Flemington, Australia)

with a diameter of 15 µm and a depth of 10 µm and in-house constructed cylindrical microwells with a diameter of 30 µm and depth of 30 µm as well as a diameter of 50 µm and depth of 50 µm. Figure 3A shows that the nanomotion of cells significantly dropped with smaller diameters. These smaller volumes most likely constrained the x-y displacement of the yeasts. Hence, we selected a 50 µm size design to continue the experiments.

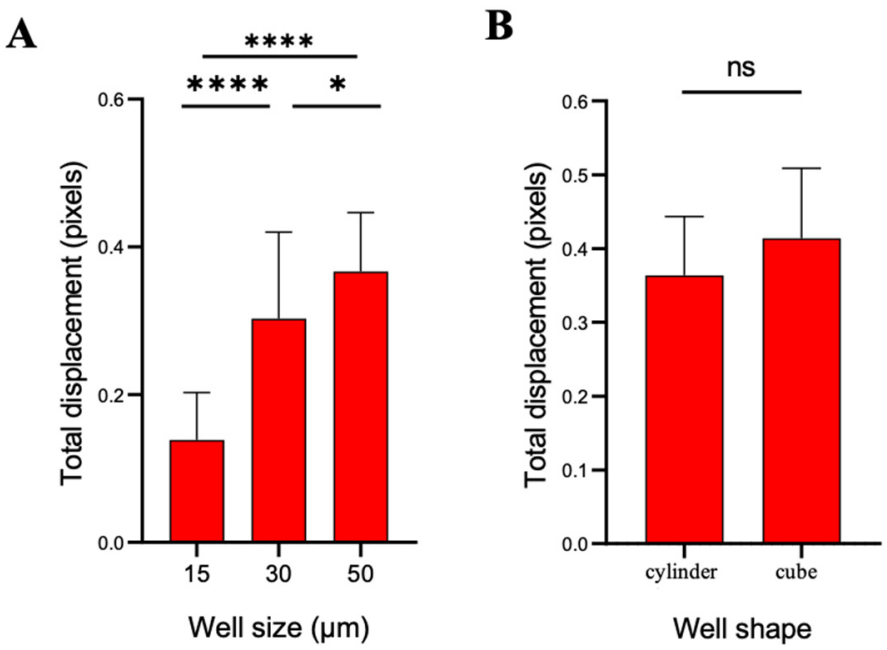

Figure 3. (**A**) Comparison of nanomotion signal between 3 different diameters of cylindrical mi crowells (15 µm, 30 µm and 50 µm) (n = 26). (**B**) Comparison of nanomotion signal between cylindrical (50 × 50 µm) and rectangular (50 × 50 × 50 µm) microwells (n = 26). Wilcoxon test: **** $p < 0.0001$; * $p < 0.1$; ns: not significant.

Besides the size, we evaluated the optimum shape of the well too. We considered two shapes: a cylindrical and cubic shape, where the diameter/sides of the wells were equal to the depth of the wells. There was not a significant difference in nanomotion between the two shapes (Figure 3B), but the volume of the cubic wells was larger than cylindrical wells, which provided the cells with more room for nanomovements as well as undisturbed growth.

3.1.2. Microfluidic Chip Design and Modelling of Fluid Flow and Mass Transport

The microfluidic chip was designed to enable the easy exchange of liquids without flushing out the cells that were trapped in the microwells. We simulated the fluid flow in a microwell (cubic with a width of 50 µm and a depth of 50 µm) in the Ibidi channel (Figure 4), using the flow rate to exchange the growth medium with the medium containing the antifungal. The calculated velocity field is shown in Figure 4A. The laminar flow in the channel induced a vortex in the microwell, as shown by drawing the streamlines (Figure 4B,C). Additionally, this was confirmed by simulating the circular movement of a yeast cell in the microwell upon fluid flow in the channel (Figure 4E–H and Video S1). It could also be observed (Figure 4G) that a cell that flowed over the microwell was initially attracted to the microwell before it was next repelled.

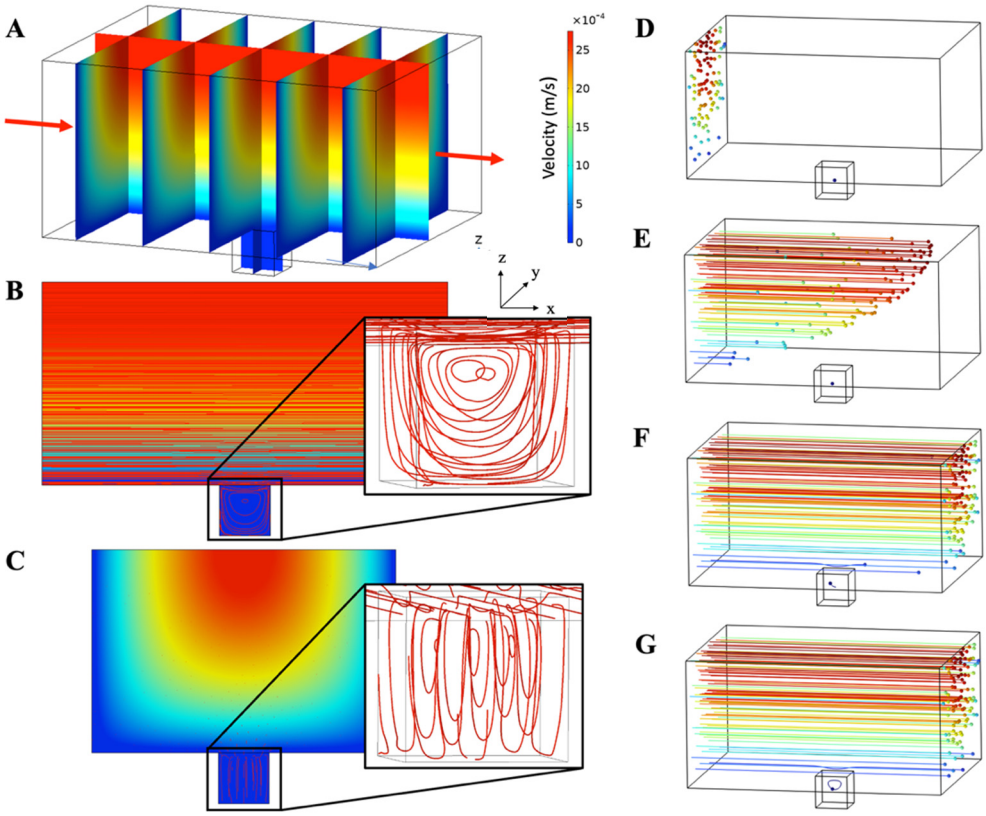

Figure 4. (**A**) Simulation of the velocity field in the channel and the microwell for an inlet flow velocity of 1.32 10^{-3} m/s. The top surface is the symmetry plane of the channel (middle plane of the channel at 200 µm). (**B**) Zx cross-section showing the velocity field and the streamlines (red colour). The insert shows a zoom of the microwell in 3D with the streamlines represented as tubes. (**C**) Zy cross-section showing the velocity field and the streamlines (red colour). The insert shows a zoom of the microwell in 3D with the streamlines represented as tubes. (**D**–**G**) Simulation of the flow of yeast cells with a flowing medium in the channel and the circular movement of a yeast cell in the microwell at (**D**) 0.00 s, (**E**) 0.13 s, (**F**) 0.8 s, and (**G**) 3.7 s (the colours of the streamlines correspond to the magnitude of the velocity, as shown in the scale bar of (**A**)) (see also Video S1).

The trapping of the cell in the microwells was experimentally confirmed by observing the movement of the cell during an exchange of the medium with an antifungal solution (Video S2). We observed that a yeast cell did not leave the well, even if there was a continuous flow (flow rate of 120 µL/min) in the channel above (Figure 5). The cell circled inside the well and went in and out of focus depending on its position in the well.

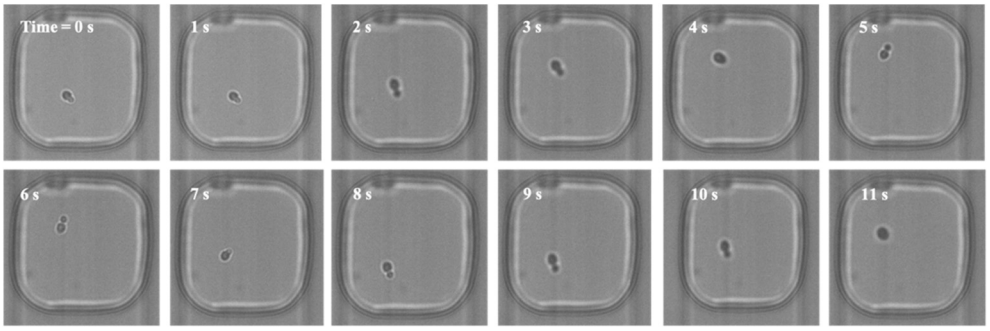

Figure 5. Progression of the circular movement of the yeast cell in the microwell during the continuous flow of liquid in the channel at a flow rate of 120 µL/min (see also Video S2).

To determine how fast the mixing in a microwell occurred when a solution flowed over the well, we observed the increase in the fluorescence of the microwell when a fluorescent solution flowed over the microwell. The evolution of the fluorescence was recorded in the middle of the well and then in the channel 200 µm above the well (Figure S1). The two data sets were normalized and plotted. We observed no difference in the increase in fluorescence between the two spots when the fluorescent solution flowed at a flow rate of 120 µL/min (Figure 6A–C). The same experiment was repeated with a lower flow rate of 10 µL/min. Here, we could observe a delay in the increase in the fluorescence of the well compared to its position on the channel (Figure 6B–D).

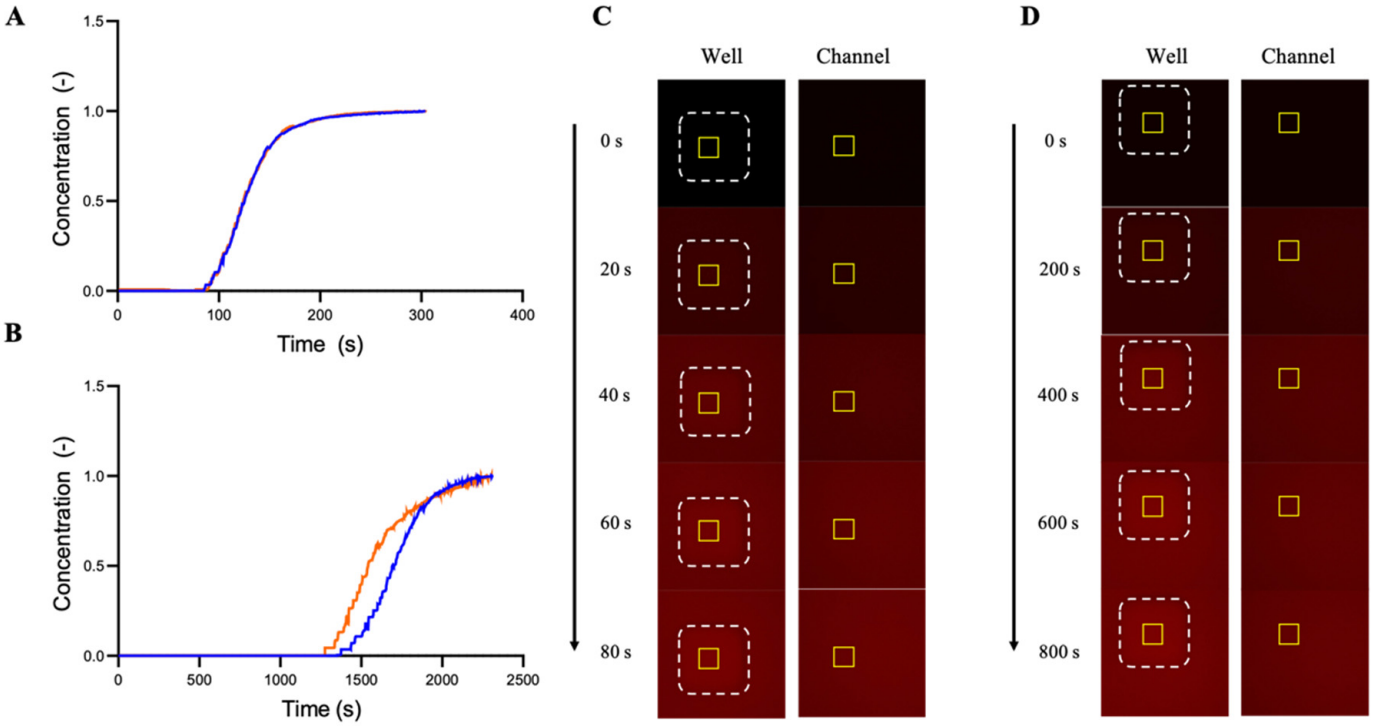

Figure 6. (**A**) Evolution of experimentally determined PI concentration in the well (blue) and middle of the channel (orange) at a flow rate of 120 µL/min (**B**) Evolution of the experimentally determined PI concentration in the well (blue) and middle of the channel (orange) at a flow rate of 10 µL/min. (**C**) Mixing of PI in the chip at a flow rate of 120 µL/min: fluorescent images at different time points; yellow squares represent the analysed area and white dashed squares indicate the edges of the well. (**D**) Mixing of PI in the chip at a flow rate of 10 µL/min: fluorescent images at different time points; yellow squares represent the analysed area. The time point of 0 s in C and D corresponds to the timepoint at which the intensity curves started to increase in A and B.

To analyse the nanomotion of the same cell over a certain period, the cells must be at a distance apart to avoid any physical contact that could interfere with nanomotion measurements. Practically, it means that the optimal distribution is one or two cells per well. The chip was filled with cell suspension at a flow rate of 120 µL/min. Analysing 275 wells, we observed that 21% of the wells were empty, 31% were filled with a single cell, 24% were filled with two cells, 12% were filled with three cells, and 12% were filled with more than three cells. Finally, 55% of the wells were optimally filled, i.e., one or two cells were present in a well (Figure 7A,B).

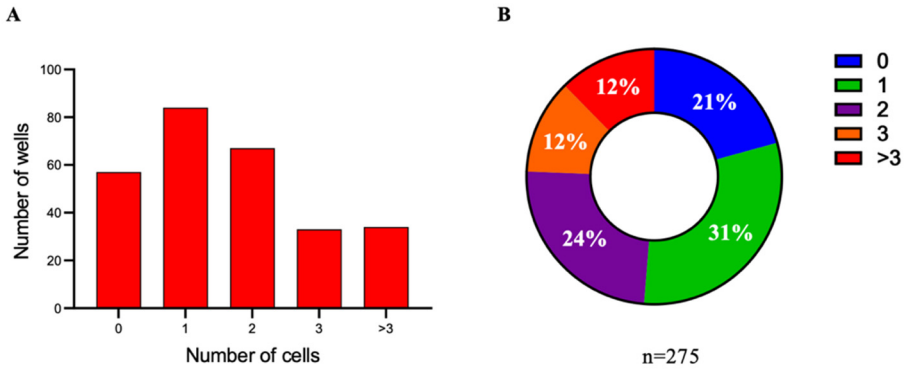

Figure 7. (**A**) The number of cells/well for n = 275 wells. (**B**) Percentage (%) of empty microwells, 1 cell/well, 2 cells/well, 3 cells/well, and more than 3 cells/well (Figure S2).

3.2. Cell Nanomotion and Susceptibility for the Antifungals Caspofungin and Fluconazole

The microfluidic chip permits not only monitoring single cells in different wells but also analysing more cells per experiment. Caspofungin experiments were conducted on two different *C. albicans* strains: a wild-type strain (CAF2-1) that was sensitive to caspofungin and fluconazole, and an azole hypersusceptible strain (DSY1024) that was documented to be inactivated with lower concentrations of azole antifungals since, in this strain, efflux genes were deleted [42]. We also evaluated the susceptibility of the DSY1024 strain against caspofungin.

3.2.1. *C. albicans* CAF2-1 Susceptibility for Caspofungin

As a control experiment, we first measured the nanomotion of 20 individual yeast cells of *C. albicans* CAF2-1 during their growth in a YPD medium over a period of 120 min. As shown in Figure 8A, Figure 9A, and Figure S3, there was no significant difference in the total displacement of all cells between 0 min and 120 min of growth.

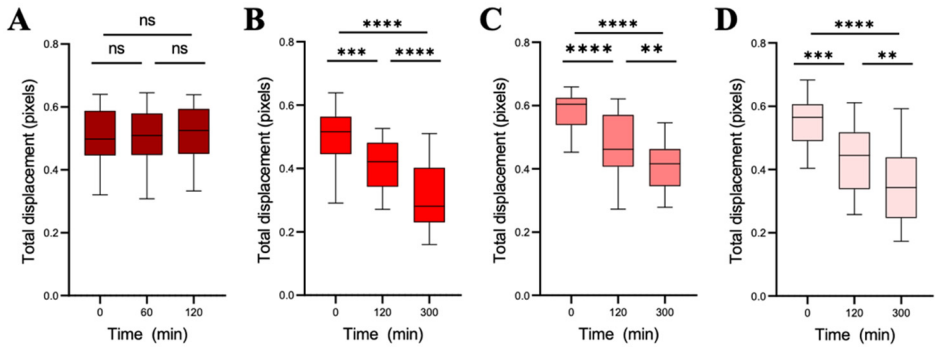

Figure 8. The average cellular nanomotion of 20 cells of *C. albicans* CAF2-1 wild-type strain. The total displacement of 20 cells was analysed during (**A**) 2 h of growth in a YPD medium (control) and during 5 h of caspofungin treatment at (**B**) 0.5 µg/mL, (**C**) 1 µg/mL, and (**D**) 100 µg/mL. Wilcoxon test: **** $p < 0.0001$; *** $p < 0.001$; ** $p < 0.01$; ns: not significant.

Next, we evaluated the effect of caspofungin on *C. albicans* CAF2-1 cells (i.e., the wild-type strain susceptible to caspofungin). Single-cell displacements were recorded every 60 min for 300 min. We used different concentrations of the antifungal compound, i.e., 0.5 µg/mL, 1 µg/mL, and 100 µg/mL. Reported MIC values of caspofungin for the strain CAF2-1 were 0.06 µg/mL [50] and 0.03 µg/mL [51] as well as the general range for *C. albicans* 0.06 µg/mL–2 µg/mL [52]. For all three concentrations, a significant decrease in the cellular displacements and total displacement was detected as soon as 2 h of treatment had elapsed (Figure 8B–D, Figure S4). The most significant drop in nanomotion after 2 h of treatment was observed using a concentration of 1 µg/mL (Figure 8C). Both 100 µg/mL

and 0.5 μg/mL caspofungin treatments also caused a significant reduction in nanomotion after 2 h (Figure 8B,D).

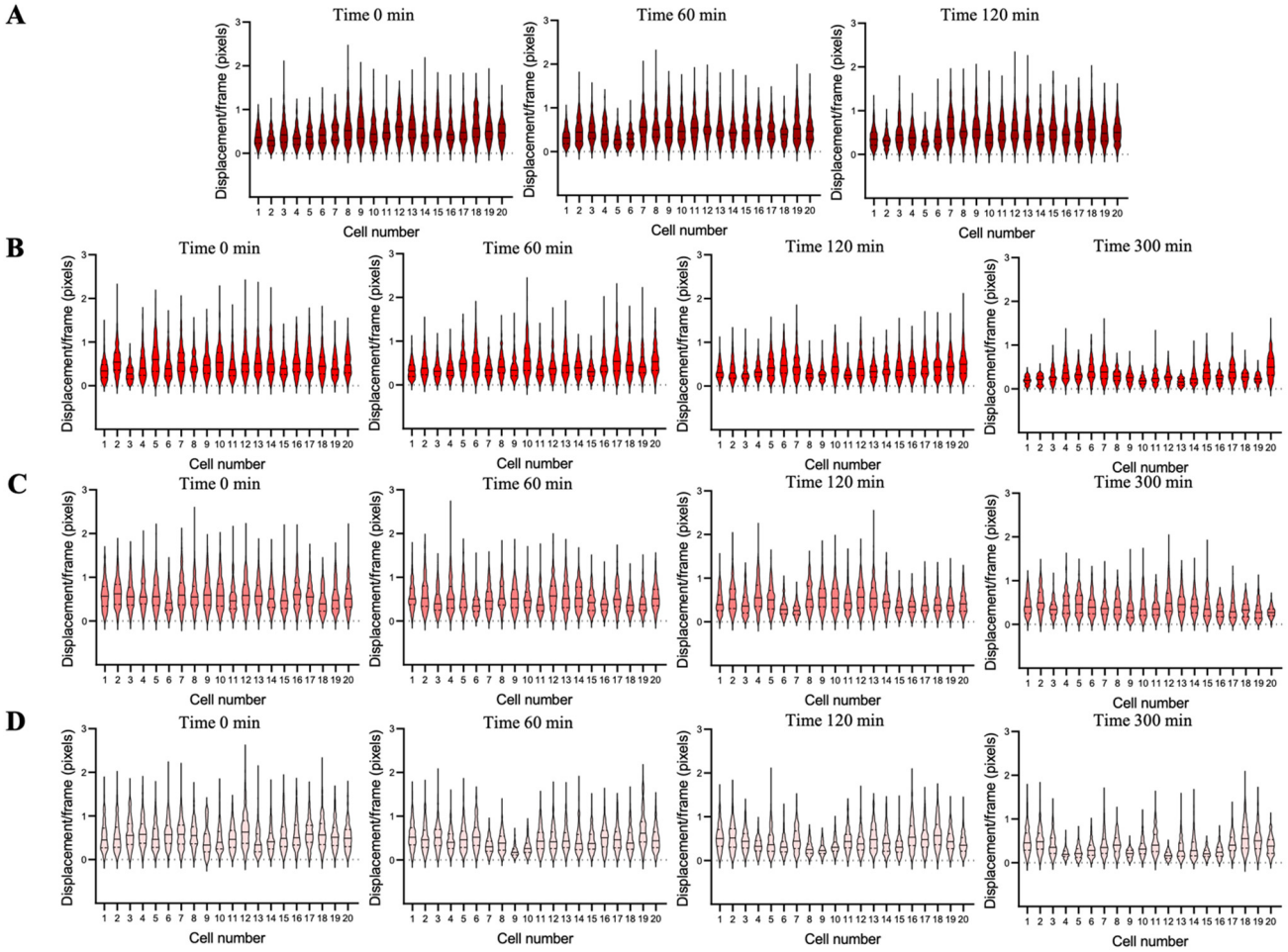

Figure 9. The displacement distribution for 20 single cells of *C. albicans* CAF2-1 wild-type strain displayed in violin plots during (**A**) 2 h of growth in a YPD medium (control) and during 5 h of treatment with the antifungal caspofungin at (**B**) 0.5 μg/mL, (**C**) 1 μg/mL, and (**D**) 100 μg/mL.

While observing the effect of 0.5 μg/mL antifungal treatment on a population of the CAF2-1 strain at a single cell level, we noticed that cells 4, 6, 15, and 20 (Figure 9B) still showed nanomotion after 300 min where the rest of the population had a significant drop, as illustrated by cells 1, 10, and 12 (Figure S5). At the single cell level at 1 μg/mL antifungal treatment after 300 min, we observed a drastic drop in almost all the cells in the population (Figure 9C). Cells 8, 9, and 10 (Figure 10 and Figure S6) presented a similar drop in nanomotion from 10 min after treatment. Looking at the single cell level at 100 μg/mL of antifungal treatment, we observed that cells 1, 2, 18, and 19 (Figure 9D) had a less drastic drop in nanomotion after 300 min in comparison to other cells in the population. Furthermore, in the separately represented cells 5, 10, and 12 (Figure S7), we could observe a difference in the nanomotion drop over the period. Cell 10 had a nearly linear drop in contrast to the other two cells, where the nanomotion dropped down almost immediately (after 10 min) and fluctuated over time.

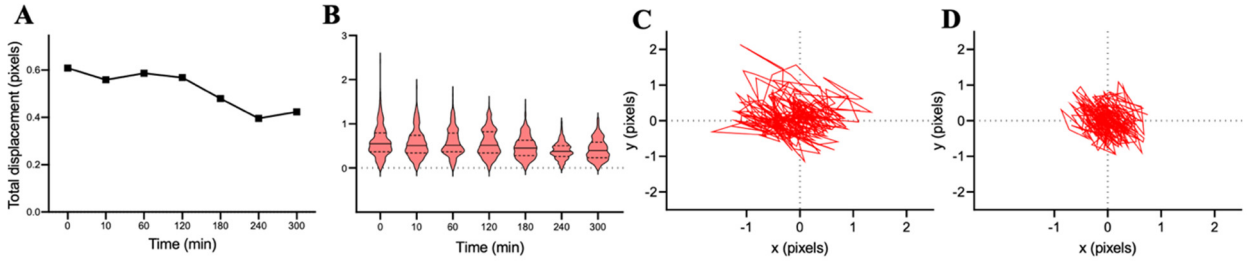

Figure 10. Effect of antifungal caspofungin (1 µg/mL) on the cellular nanomotion of cell 8 from Figure 9C (*C. albicans* CAF2−1). (**A**) Total displacement (pixels) as a function of time for cell 8 (see also a movie of cell 8 that was recorded before treatment (Video S3) and at 10 min (Video S4). (**B**) Distribution of the displacement/frame as a function of time for cell 8. (**C**) X−y displacement of cell 8 before treatment, time point 0 min). (**D**) X−y displacement of cell 8 after 300 min of treatment.

3.2.2. *C. albicans* CAF2-1 Susceptibility for Fluconazole

We evaluated the effect of fluconazole on *C. albicans'* CAF2-1 cells. Single-cell displacements were recorded every 60 min for 300 min. We used antifungal concentrations of 0.5 µg/mL, 1 µg/mL, and 100 µg/mL. A reported MIC value of fluconazole for the strain CAF2-1 was 0.25 µg/mL [53]. For all three concentrations, a significant decrease in cellular displacements and the total displacement was detected as soon as after 2 h of treatment (Figure 11B–D, Figure S8). The most significant drop in nanomotion after 2 h of treatment was observed using a concentration of 100 µg/mL (Figure 11D). Both 0.5 µg/mL and 1.0 µg/mL fluconazole treatments also caused a significant reduction in nanomotion after 2 h (Figure 11B,C).

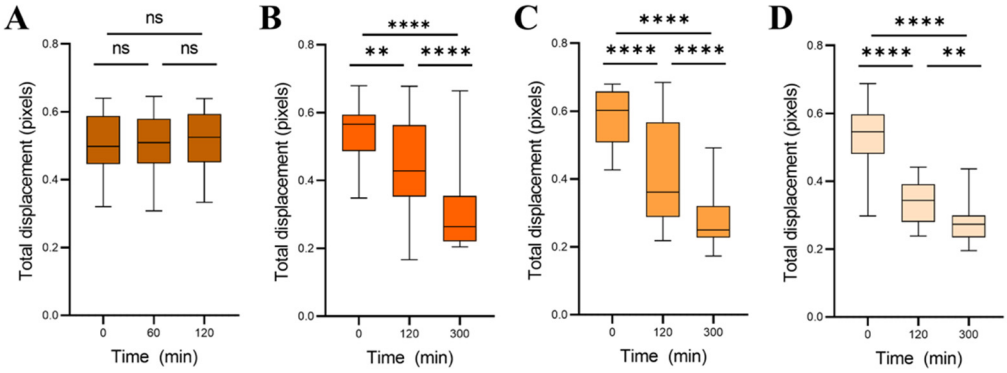

Figure 11. The average cellular nanomotion of 20 cells of *C. albicans* CAF2-1 wild-type strain. The total displacement of 20 cells was analysed during (**A**) 2 h of growth in a YPD medium (control) and during 5 h of fluconazole treatment at (**B**) 0.5 µg/mL, (**C**) 1 µg/mL, and (**D**) 100 µg/mL. Wilcoxon test: **** $p < 0.0001$; ** $p < 0.01$; ns: not significant.

While observing the effect of 0.5 µg/mL antifungal treatment on a population of the CAF2-1 strain at a single cell level, we noticed that cells 4, 9, 13, and 16 (Figure 12B) still showed nanomotion after 300 min where the rest of the population experienced a significant drop. In cells 5, 6 and 7, we observed that the nanomotion signal starts dropping after 10 min of treatment (Figure S9). At the single cell level at 1 µg/mL antifungal treatment after 300 min, we observed a drop in nanomotion except for cells 8, 12, and 13 (Figure 12C). Furthermore, in the separately represented cells 17 (Figure 13), 18, and 19 (Figure S10), we could observe a difference in nanomotion drop over the period. Cell 17 and 19 had a nearly linear drop in contrast to cell 18, where the nanomotion dropped down after 2 h. For treatment with 100 µg/mL antifungal treatment, we observed a significant drop in all the cells (Figure 11D, Figure S11).

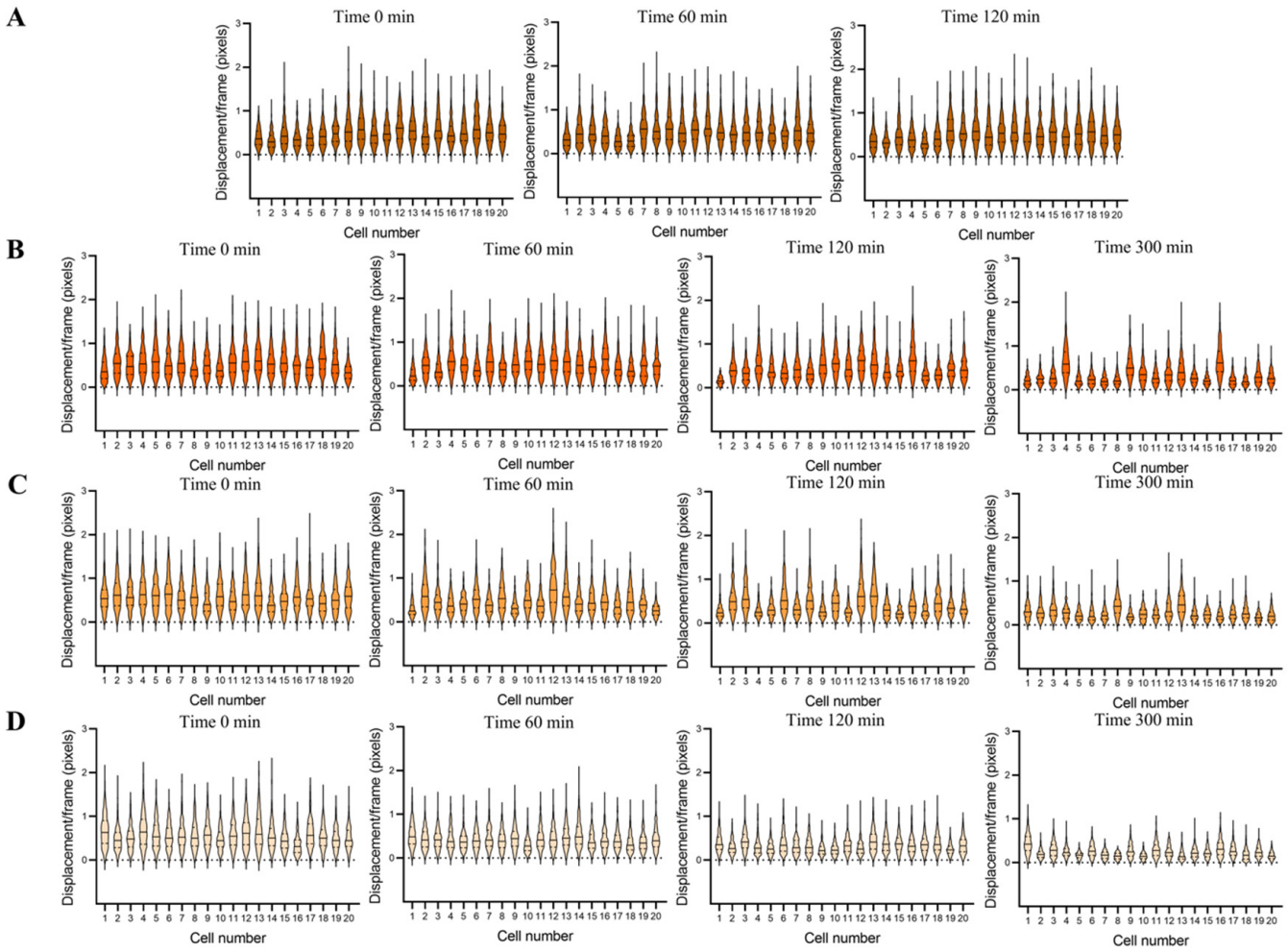

Figure 12. The displacement distribution for 20 single cells of *C. albicans* CAF2-1 wild-type strain displayed in violin plots during (**A**) 2 h of growth in a YPD medium (control) and during 5 h of treatment with the antifungal fluconazole at (**B**) 0.5 μg/mL, (**C**) 1 μg/mL, and (**D**) 100 μg/mL.

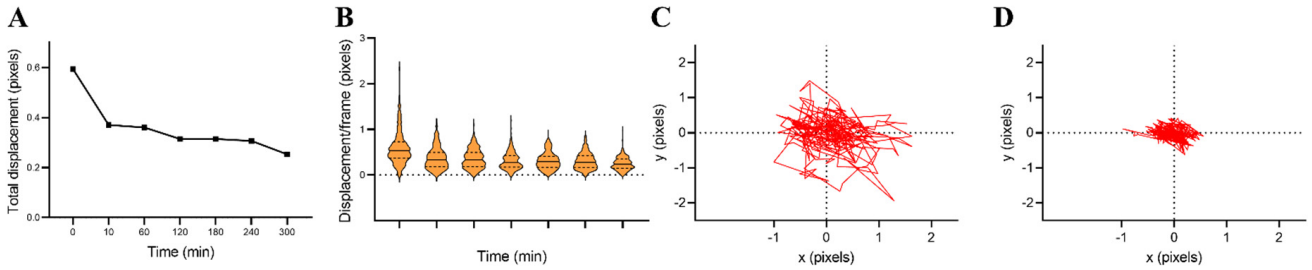

Figure 13. Effect of the antifungal fluconazole (1 μg/mL) on the cellular nanomotion of cell 17 with *C. albicans* CAF2−1. (**A**) Total displacements (pixels) as a function of time for cell 17. (**B**) Distribution of the displacement/frame as a function of time for cell 17. (**C**) X−y displacement at the time point 0 min for cell 17. (**D**) X−y displacement at the time point 300 min for cell 17.

3.2.3. *C. albicans* DSY1024 Susceptibility for Caspofungin and Fluconazole

As a control experiment, the cellular nanomotion of 20 individual yeast cells of the hypersusceptible *C. albicans* DSY1024 strain was monitored during 2 h of growth in a YPD medium. There was no significant difference in the total displacement of all the cells between 0 min and 120 min of growth (Figure 14A, Figure S12).

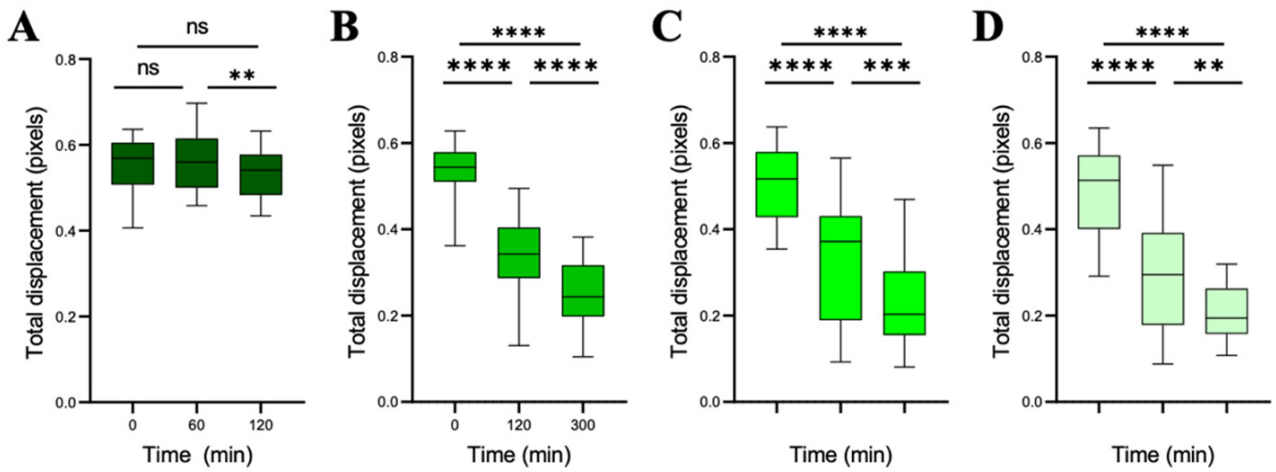

Figure 14. The average cellular nanomotion of 20 cells of *C. albicans* azole hypersusceptible DSY1024 strain treated with fluconazole. The total displacement of 20 cells was analysed during (**A**) 2 h of growth in a YPD medium (control) and during 5 h of fluconazole treatment at (**B**) 0.5 μg/mL, (**C**) 1 μg/mL, and (**D**) 100 μg/mL. Wilcoxon test: **** $p < 0.0001$; *** $p < 0.001$; ** $p < 0.01$; ns: not significant.

ONMD of *C. albicans* DSY1014 Treated with Fluconazole

The susceptibility of the azole hypersusceptible DSY1024 strain for fluconazole treatment was assessed. A reported MIC value of fluconazole for the strain DSY1024 was 0.03 μg/mL [53]. During the treatment with different concentrations of fluconazole, i.e., 0.5 μg/mL, 1 μg/mL, and 100 μg/mL, we observed a significant decrease in the cellular displacements and total displacement (Figure 14B–D, Figure 15B−D, Figure S13) compared to the control (Figure 14A). All 20 cells that were analysed showed a drastic drop in nanomotion after 300 min of treatment with 0.5 μg/mL fluconazole, which indicated that this strain was susceptible to this concentration (Figure 15B, Figure S14). While treating the strain DSY1024 with 1 μg/mL of fluconazole, we observed that after both 120 min and 300 min, all the cells in the population reduced their nanomovements (Figure 15C, Figure S15). In cell 1, we observed as well a drop in the nanomotion (Figure 16). During the treatment with 100 μg/mL fluconazole, we observed that all cells after 300 min had a significant drop in their nanomotion (Figure 15D, Figure S16).

ONMD of *C. albicans* DSY1014 Treated with Caspofungin

The susceptibility of the azole hypersusceptible DSY1024 strain for caspofungin was assessed. During the treatment with different concentrations of caspofungin, i.e., 0.5 μg/mL, 1 μg/mL, and 100 μg/mL, we observed a significant decrease in the cellular displacements and total displacement (Figure 17B–D, Figure 18B−D, Figure S17) as well as in the x-y displacement (Figure 19). Using a caspofungin concentration of 1 μg/mL, we observed the most significant drop over a period of 5 h (Figure 17C). Both responses to 100 μg/mL and 0.5 μg/mL treatments were significant even after 2 h (Figure 17B,D) but were less in comparison to 1 μg/mL.

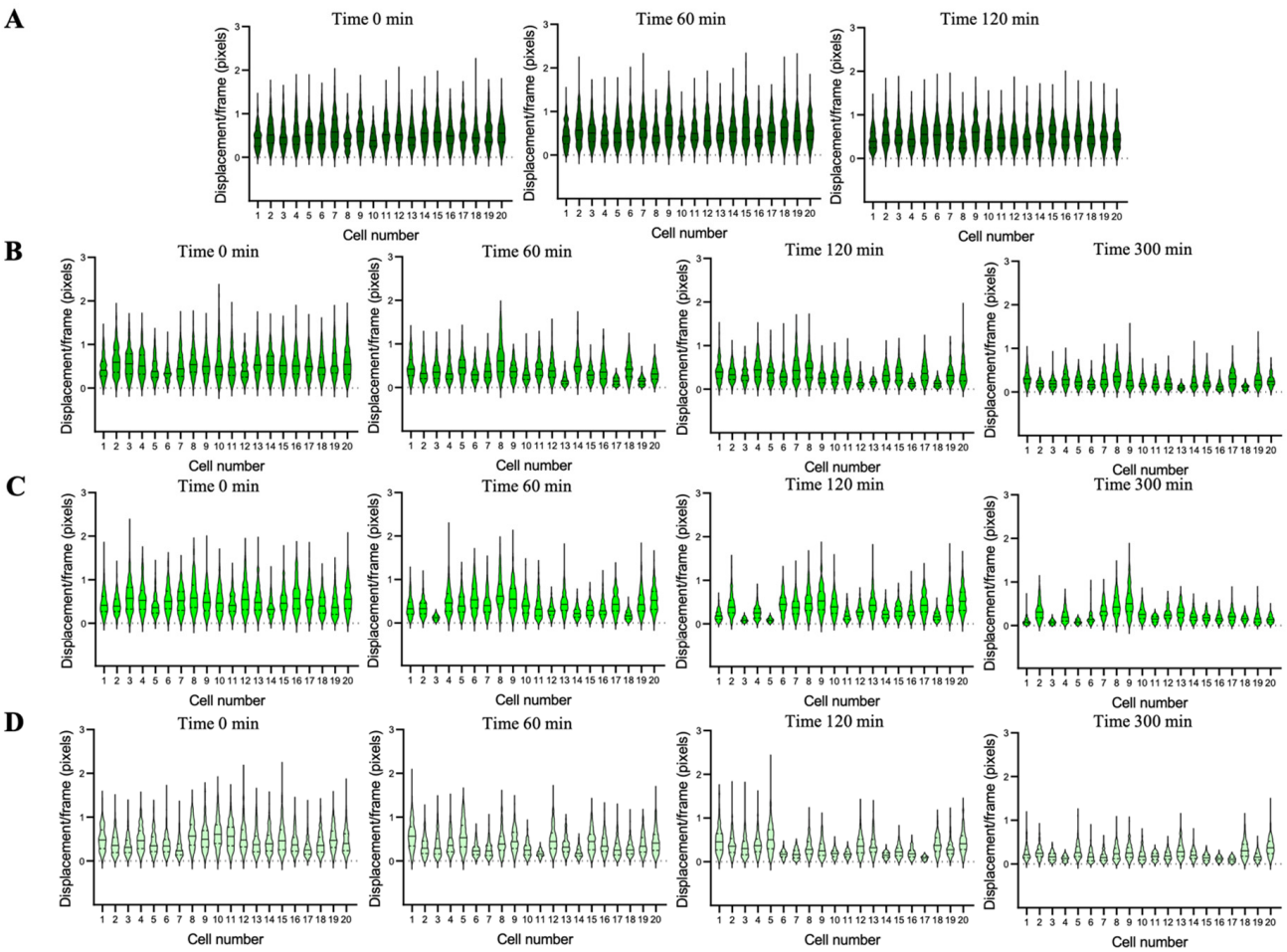

Figure 15. The displacement distribution for 20 single cells of *C. albicans* DSY1024 strain displayed in violin plots during (**A**) 2 h of growth in a YPD medium (control) and during 5 h of treatment with the antifungal fluconazole at (**B**) 0.5 µg/mL, (**C**) 1 µg/mL, and (**D**) 100 µg/mL.

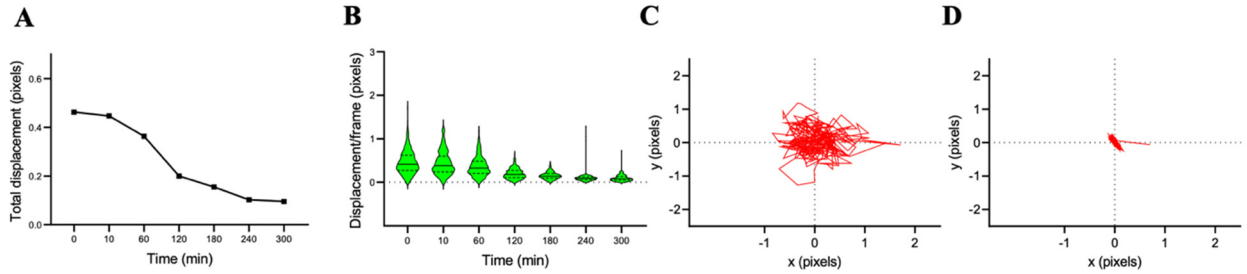

Figure 16. Effect of the antifungal fluconazole (1 µg/mL) on the cellular nanomotion of cell 1 from *C. albicans* DSY1024. (**A**) Total displacement (pixels) as a function of time for cell 1 (**B**) Distribution of the displacement/frame as a function of time for cell 1. (**C**) X−y displacement of cell 1 before treatment time point 0 min. (**D**) X−y displacement of cell 1 after 300 min of treatment.

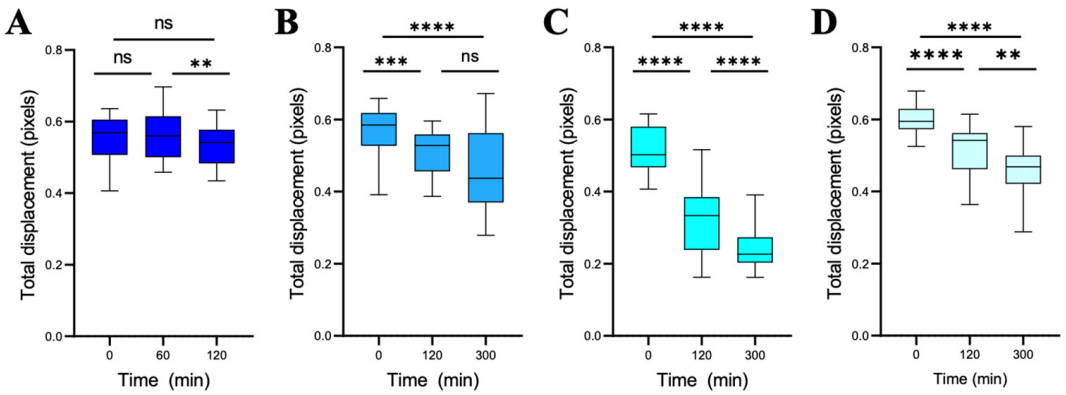

Figure 17. Average cellular nanomotion for 20 cells of *C. albicans* DSY1024 strain treated with caspofungin. The total displacement of 20 cells was analysed during (**A**) 2 h of growth in a YPD medium (control) and during 5 h of caspofungin treatment with (**B**) 0.5 μg/mL, (**C**) 1 μg/mL, and (**D**) 100 μg/mL. Wilcoxon test: **** $p < 0.0001$; *** $p < 0.001$; ** $p < 0.01$; ns: not significant.

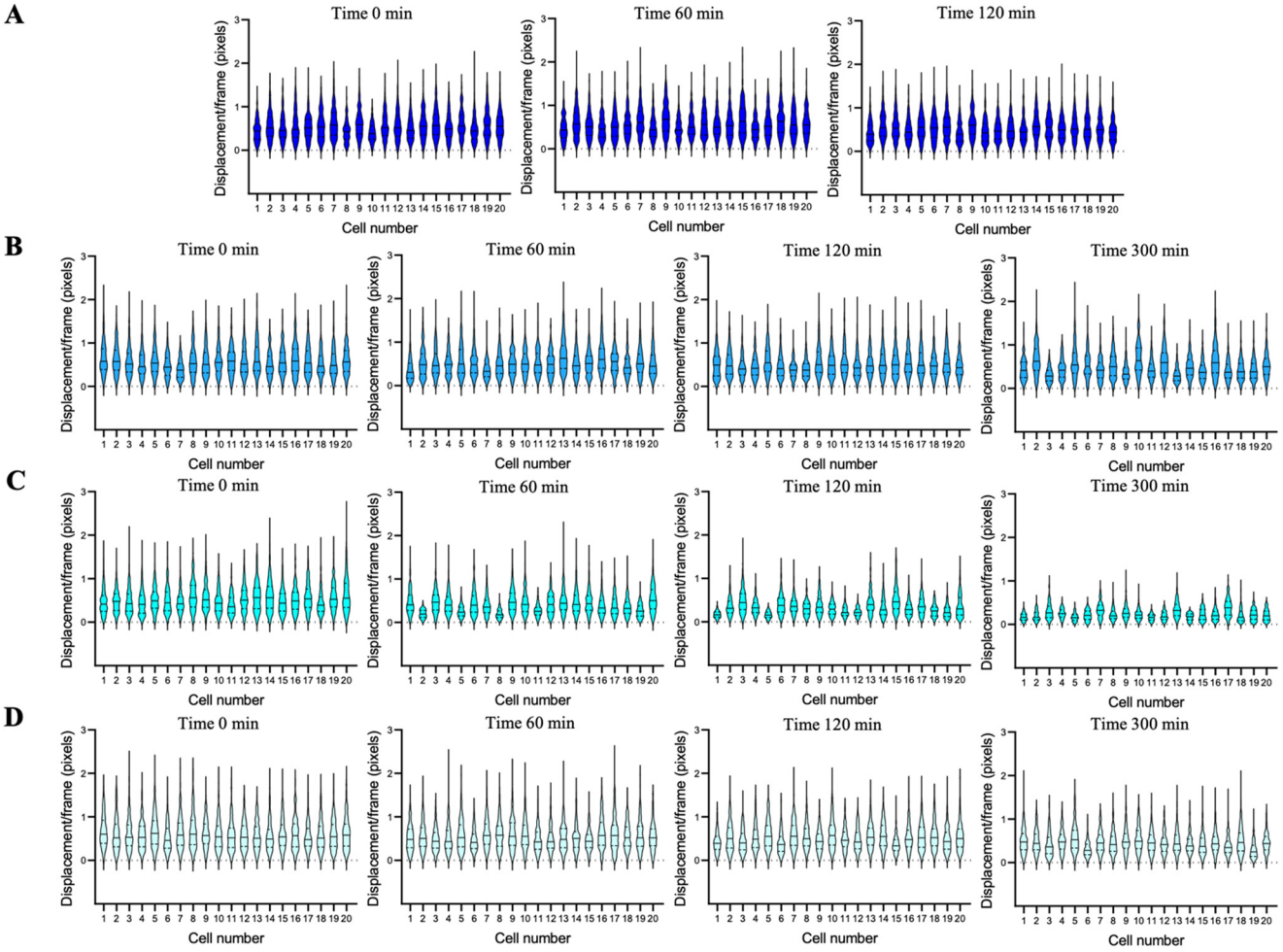

Figure 18. The displacement distribution for 20 single cells of *C. albicans* DSY1024 strain displayed in violin plots during (**A**) 2 h of growth in a YPD medium (control) and during 5 h of caspofungin treatment with (**B**) 0.5 μg/mL, (**C**) 1 μg/mL, and (**D**) 100 μg/mL.

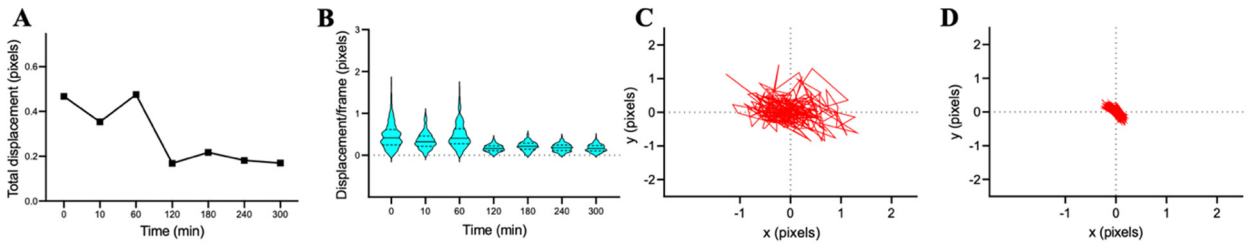

Figure 19. Effect of antifungal caspofungin (1 μg/mL) on the cellular nanomotion of cell 1 in Figure 12 C (*C. albicans* DSY1024). (**A**) Total displacements (pixels) as a function of time for cell 1. (**B**) Distribution of the displacement/frame as a function of time for cell 1. (**C**) X-y displacement of cell 1 before treatment. (**D**) X-y displacement at the time point of 300 min for cell 1.

In the population of strain DSY1024, half of the cells (cells 2, 5, 6, 7, 8, 10, 12, 15, and 16) (Figure 18B) still showed nanomovements after 300 min of treatment with 0.5 μg/mL of caspofungin, which indicated that these cells were more tolerant to this concentration of the antifungal, as represented by cell 12 (Figure S18), for which we observed an increase in nanomotion over the period. On the other hand, the rest of the cells had a significant drop in nanomotion, as represented by cells 3 and 14 (Figure S18).

After treating the strain DSY1024 with 1 μg/mL of caspofungin, we observed that after both 120 min and 300 min, all the cells in the population reduced their nanomovements (Figure 18C), and the drop was greater than in the population of the wild-type strain (Figure 9C). Furthermore, for the separately represented cell 1, we observed a large drop after 120 min, which did not change much for the next 2 h. Cells 9 and 13 experienced a more gradual drop (Figure S19). While observing the single-cell nanomotion of strain DSY1024 during the treatment with 100 μg/mL caspofungin, we observed that many cells after 300 min stayed with similar nanomovements as before the treatment (Figure 18D). The separately represented cells 2, 6, and 19 (Figure S20) were quite diverse in their response to a high concentration of caspofungin. Cell 2 had a slight drop in nanomotion in contrast to cells 6 and 19, where the drop was more drastic.

3.2.4. Sensitivity Analysis Based on the Evolution of the Slopes of the Total Displacements

The sensitivity of the individual *Candida* cells to caspofungin was characterized by analyzing the slope of their decrease in nanomotion activity (total displacement) as a function of time. We calculated the slopes of the total displacement as a function of time for 10, 60, 120, 180, 240, and 300 min after the treatment with 0.5 and 1 μg/mL caspofungin for the wild-type CAF2-1 strain (Figure 20A, Figure S21) and the hypersusceptible DSY1024 strain (Figure 20C, Figure S21C), as well as the treatment with 0.5 and 1 μg/mL fluconazole for the wild-type CAF2-1 strain (Figure 20B, Figure S21B) and the DSY1024 strain (Figure 20D, Figure S21D). The more sensitive the cells were to caspofungin or fluconazole, the steeper the slopes were. The decreases in the slopes of the hypersusceptible strain, when treated with 0.5 μg/mL of fluconazole, were significantly larger than the ones treated with caspofungin as well as the caspofungin treatment of the wild-type strain. The largest slopes were recorded 10 min or 60 min after the treatment and, in the case of the fluconazole treatment of the DSY1024 strain, this slope was the largest, which clearly demonstrates that this strain was hypersusceptible to fluconazole. Based on these results, we can conclude that the values of these slopes enable the effect of a killing compound to be quantified in a short time frame (10 to 60 min). The evolution of the average slopes for the 20 cells showed that the slope values decreased as a function of time (Figure 20A–D, Figure S21A–D), and the slope value at 10 min of treatment already gave an indication of the susceptibility of the strain. The calculation of the slopes for the control experiment (without antifungal treatment) showed fluctuating negative—positive values for the CAF2-1 strain (Figures 20E and 21F) and the DSY1024 strain (Figures 20E and 21F). The nanomotion analysis results the total displacements as a function of time indicate that this wild-type

strain was somewhat more susceptible to caspofungin than to fluconazole (Figure 21A,C and Figure S22).

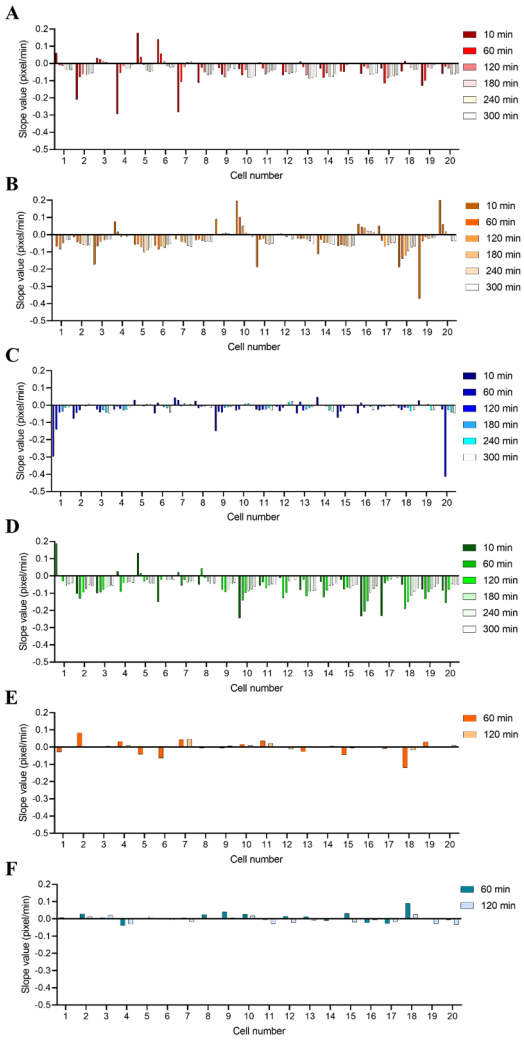

Figure 20. The slopes of the decrease in the total displacement of 20 cells as a function of time were calculated based on the time points 10, 60, 120, 180, 240, and 300 min during 0.5 µg/mL caspofungin or fluconazole treatment of the *C. albicans* strains: (**A**) Caspofungin-treated CAF2−1, (**B**) Fluconazole-treated CAF2−1, (**C**) Caspofungin-treated DSY1024, (**D**) Fluconazole-treated DSY1024 during the 2 h growth in YDP medium (**E**) CAF2−1 and (**F**) DSY1024.

3.3. Cellular Nanomotion of Living Cells Compared to Dead Cells

We performed single-cell nanomotion measurements on living cells and compared the data to the measurements on dead cells that were killed using 70% (*v*/*v*) ethanol and 1 h of incubation. Living cells were characterised by a median total displacement of 0.51 (pixels), whereas dead cells had a median total displacement of 0.06 (pixels) (Figure S23. The viability of the cells was determined using PI staining just before the nanomotion measurements as 100% and 0% after 1 h treatment with ethanol (Figure S23B).

4. Discussion

Nanomotion is a sensitive and rapid label-free technique that assesses the viability of living microbial cells [40]. Therefore, it is very well suited to conduct rapid antifungal susceptibility testing. It was demonstrated that the nanomotion of yeast cells could be linked to their metabolic state by comparing the nanomotion signal of cells that grew in the presence of sufficient nutrients to cells that lacked nutrients and by detecting a

maximal cellular nanomotion at the optimal growth temperature [40]. Here, we developed a microfluidic chip equipped with microwells to trap and analyse the nanomotion of single cells. We selected cubic-shaped microwells (Figure 3B) with a width of 50 μm (Figure 3A) and a depth of 50 μm (giving a depth-to-width ratio of 1). The microwells trapped single cells homogenously and organized them over the microwell array. More than 50% of the wells could be filled with one or two cells, which is ideal for the performance of single-cell nanomotion analysis (Figure 7).

As confirmed by the simulations of the fluid flow in the microwells (Figure 4), these dimensions create a vortex when the liquid is flown over the microwell (Figure 5 and Video S1). Previously, it was demonstrated that a vortex was created in a microwell when the depth-to-width ratio equalled one or was larger than one [54]. The vortex traps the cell in the microwell and allows the quick mixing of the antifungal upon liquid exchange. In our analysis, the convective mixing time at a high flow rate (120 μL/min) was less than 2 min and did not differ between the mixing time in the channel (Figure 6). Such a fast-mixing time allowed us to record the nanomotion of the cells immediately after their exposure to an antifungal drug or any other chemical treatment.

We performed a series of experiments to validate the nanomotion method for cells in microwells as an efficient and rapid antifungal susceptibility test. As a first proof-of-concept experiment of the microwell ONMD method, we assessed the susceptibility of the *C. albicans* wild-type CAF2-1 strain to caspofungin. Caspofungin acetate belongs to a new class of antifungals referred to as echinocandins [55]. The effect of caspofungin is related to the inhibition of fungal cell wall synthesis by disrupting the cell wall glucan formation through the non-competitive inhibition of an enzyme complex 1,3-β-D-glucan synthase [55]. We selected two concentrations that were reported within or close to the minimal inhibitory concentration (MIC) range [52], i.e., 0.5 μg/mL and 1 μg/mL, and a large concentration of 100 μg/mL caspofungin (to obtain a fast response and to compare this response with other rapid nanonomotion-based methods [41]). For the 3 caspofungin concentrations, we observed a significant drop in nanomotion upon the injection of the antifungal in the chip (Figures 8 and 14). The caspofungin susceptibility for the MIC concentration could be demonstrated, indicating the method's high sensitivity.

Next, we assessed the susceptibility of the *C. albicans* CAF2-1 strain to fluconazole. Fluconazole, which belongs to the class of azole antifungals, has the useful characteristics of a wide antifungal spectrum, low toxic effects, and high bioavailability and is, therefore, widely used in the clinical treatment of *C. albicans* infections [56]. However, fluconazole is a fungistatic drug that inhibits growth but does not kill the pathogenic fungus, thereby providing an opportunity for the development of fluconazole resistance [57,58]. Fluconazole inhibits ergosterol biosynthesis by inhibiting the cytochrome P450–dependent lanosterol 14-α-demethylase (14DM) enzyme selectively [59]. Resistance can be caused by alterations in sterol biosynthesis, by mutations in the drug target enzyme 14DM, or by the overexpression of genes coding for the membrane transport proteins of the ABC (ATP-binding cassette) transporter (*CDR1/CDR2*) or the major facilitator (*MDR1*) superfamilies [60,61]. Different mechanisms are frequently combined, resulting in a stepwise development of fluconazole resistance over time. The nanomotion analysis results, including the variation in the slopes of the total displacements as a function of time indicate that this wild-type strain was somewhat more susceptible to caspofungin than to fluconazole (Figure 21A,C).

As a second proof-of-principle experiment, we assessed the susceptibility of the azole hypersusceptible DSY1024 strain for fluconazole and caspofungin. The *C. albicans* strain DSY1024 that was used in this study was hypersusceptible to fluconazole since the multidrug efflux transporter genes *CDR1*, *CDR2*, *CaMDR1*, and *FLU1* were deleted [42,62]. The disruption of *FLU1* in *C. albicans* had only a slight effect on fluconazole susceptibility; however, it resulted in hypersusceptibility to mycophenolic acid [62]. A significant drop in the nanomotion signal was observed after 2 h of the treatment of the DSY1024 strain with 0.5 μg/mL, 1 μg/mL, or 100 μg/mL fluconazole (Figures 13 and 14). The decrease in the nanomotion signal was significantly larger for the treatment with 0.5 μg/mL

and 100 µg/mL fluconazole compared to the treatment with the same concentrations of caspofungin (Figure 17, Figure 18, and Figure S24). There was no significant difference at the concentration of 1 µg/mL. However, the spread of the total displacement values for 1 µg/mL fluconazole treatment was significantly larger than the spread for caspofungin treatment (Figure S24B). Previously we showed that at antifungal concentrations that were close to the MIC range, the nanomotion signal increased [40]. These results confirm that DSY1024 was hypersusceptible to fluconazole [39].

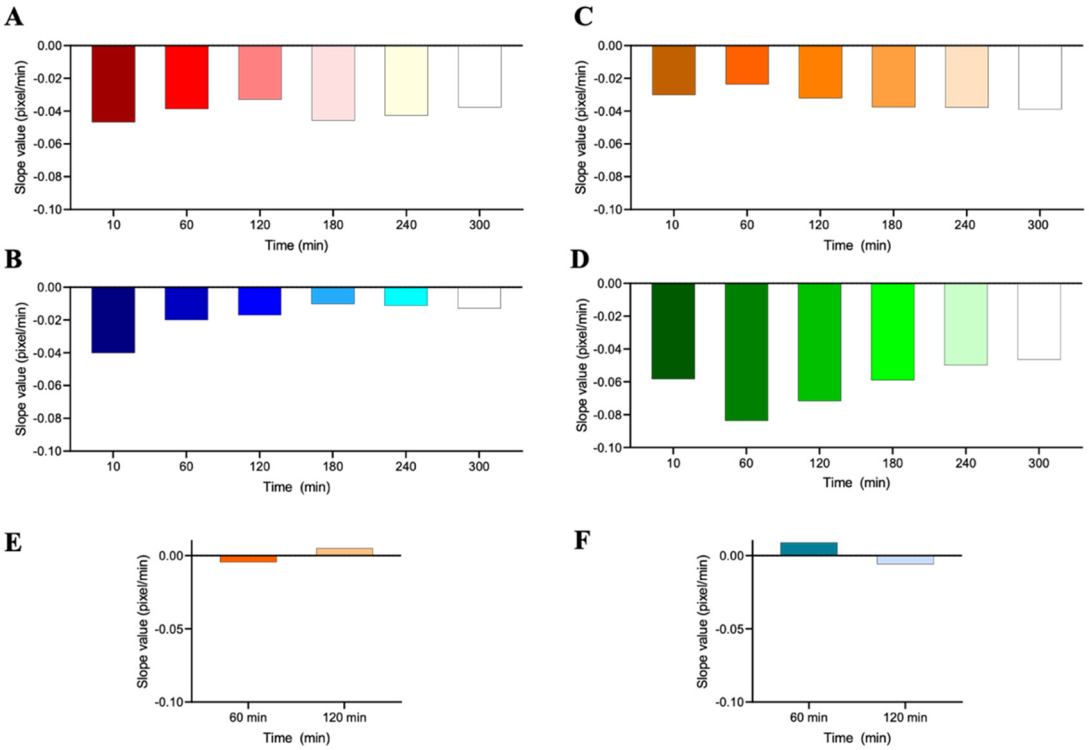

Figure 21. The slopes of the decrease in the total displacement as a function of time are calculated based on the time points 10, 60, 120, 180, 240, and 300 min during 0.5 µg/mL caspofungin or fluconazole treatment for the averages of the total displacements of all 20 cells: (**A**) Caspofungin-treated CAF2-1, (**B**) Caspofungin-treated DSY1024, (**C**) Fluconazole-treated CAF2-1, (**D**) Fluconazole-treated DSY1024 during the 2 h growth in YDP medium of (**E**) CAF2-1 and (**F**) DSY1024.

The slope of the decrease in nanomotion activity (as measured by the total displacement of the cell) as a function of time provided information on how fast the cell reacted to a specific chemical compound (Figure 20, Figure 21, Figure S21, and Figure S22) [41]. With this type of signal analysis, we highlighted the sensitivity and difference in sensitivity between the 2 *Candida* strains in as fast as 10 min. The slope for the decrease in the total displacement after 10 min or 60 min was much larger in the case of the 0.5 µg/mL fluconazole treatment of the hypersusceptible DSY1024 strain, confirming the azole hypersusceptible characteristic of this strain.

We compared the cellular nanomotion signals of living *C. albicans* CAF2-1 cells to the ones of dead cells (Figure S23). The median value of the total displacement of 20 living cells was approximately 10 times larger: 0.51 pixels for living cells versus 0.06 pixels for dead cells. The differences in nanomotion between living and dead cells were largest when living cells were in optimal conditions, i.e., when cells were in their exponential growth phase when all essential nutrients were available and when cells were grown at their optimal pH and temperature. We demonstrated previously that the nanomotion of yeast cells [40] as well as bacteria (including *Escherichia coli* and *Lactobacillus rhamnosus*) [31,63] could be linked to their metabolic state by comparing the nanomotion signal of cells that

grow in the presence of sufficient nutrients (including the carbon source) to cells that lack nutrients. We previously showed for yeast cells that the cellular nanomotion was the largest at their optimal growth temperature [40]. The molecular or subcellular organelles that caused the cells to oscillate have not yet been studied in detail. Various processes could contribute to the nanomotion signal, including DNA replication, transcription, and translation, cytoskeleton rearrangements, ionic pump activity, and organelle transport [30]. The observed displacement of dead cells can be explained as the movement of the cells due to the Brownian motion.

A large variation in displacements can be observed for living cells (Figure 11, Figure 14, Figure 17, and Figure S23). Previously, we also observed this large variation using ONMD on single yeast cells (*Candida* and *Saccharomyces cerevisiae* strains) [40,41]. A large variation in the nanomotion of single living bacteria has also been reported previously using various nanomotion detection methods. We observed this recently for the non-motile bacteria *Staphylococcus aureus*, *L. rhamnosus,* and *Mycobacterium smegmatis* using ONMD [63]. Such a variation was observed in the nanomotion of single *E. coli* that were present in a microwell [64] or stuck to flexible graphene drums [65]. Large variations in the single-cell nanomotion of *E. coli* were loosely tethered to a glass surface and were also registered by optical microscopy [37] and plasmonic imaging [36].

Many parameters could contribute to the observed variation in the nanomotion of single bacteria. Parameters such as the spread in the metabolic status of single cells, the age of the cells, senescence, and the coexistence of cells in different moments of their cell cycle [66] can significantly affect cellular displacement. Further research is needed to evaluate the contribution of these parameters to the nanomotion behaviour of single cells.

The presence of outliners in antifungal-treated cells has also been observed previously for yeast cells [40,41] as well as for antibiotic-treated bacteria [63–65] using optical nanomotion as well as other nanomotion detection methods. A better understanding of these outliners could be obtained by studying single-cell sensitivity toward various antifungals/antibiotics with a different mode of action and in a large cell population. Future experiments also need to address the existence/occurrence of a persistent and/or a resistant sub-population.

5. Conclusions

We developed a microwell-based microfluidic chip for ONMD experiments. The microwells were integrated into a microfluidic channel, allowing us to rapidly expose the trapped yeast cells to antifungals. The method allows for the analysis of a large population of cells by conserving single-cell sensitivity. Due to the creation of a vortex in the microwell, the same cell could be observed before and after exposure to an antifungal drug or any other chemical treatment. This is a major advantage of this new method. This device permitted the performance of susceptibility testing as fast as 10 min.

In the future, a dedicated microfluidic chip could be constructed where the number of channels with microwells is increased and integrated into a chip to assess different concentrations and different antifungals. Being able to perform AST for different concentrations of antimicrobial agents can also allow us to easily determine the MICs.

This development could eventually lead to a cheap and easy operational device that can be directly implemented in hospitals or even in remote doctor's practices in developing world countries. It would allow the performance of rapid antifungal susceptibility testing in the earliest possible treatment stage in order to make the appropriate decisions for personalized effective antimicrobial therapy.

Supplementary Materials: The following supporting information can be downloaded at: https://www.mdpi.com/article/10.3390/fermentation9040365/s1, Video S1: Simulation of the movement of 100 yeast cells with the flowing medium in the channel and the circular movement of one yeast cell in the microwell due to the created fluid vortex. The scale represents the velocity (m/s); Video S2: Experimental observation of the circular movement of the yeast cell in the microwell during the continuous flow of liquid in the channel at a flow rate of 120 µL/min (movie recording at 20 fps); Video

S3: Example of the nanomotion of C. albicans CAF2-1 cell 8 in a microwell before treatment (1 μg/mL caspofungin); Video S4: Example of the nanomotion of C. albicans CAF2-1 cell 8 in a microwell after 10 min of treatment (1 μg/mL caspofungin); Figure S1. Transversal (zy) cross-section of the channel and microwell with focus plane 1 where we observed the evolution of the propidium iodide (PI) concentration in the well and focus plane 2 where we observed the evolution of the PI concentration in the channel. Figure S2. Example of a part of the microwell array showing the occupancy of the microwells by the yeast cells. Figure S3. Control experiment for the C. albicans CAF2-1 strain grown in YPD medium for 3 selected cells: cell 1, 3 and 4 (A) Total displacements (pixels) as a function of time for cell 1. (B) Distribution of the displacement/frame as a function of time for cell 1. (C) X-y displacement at the time point 0 min for cell 1. (D) X-y displacement at the time point 120 min for cell 1. (E) Total displacements (pixels) as a function of time for cell 3. (F) Distribution of the displacement/frame as a function of time for cell 3. (G) X-y displacement at the time point 0 min for cell 3. (H) X-y displacement at the time point 120 min for cell 3. (I) Total displacements (pixels) as a function of time for cell 4. (J) Distribution of the displacement/frame as a function of time for cell 4. (K) X-y displacement at the time point 0 min for cell 4. (L) X-y displacement at the time point 120 min for cell 4. Figure S3. Control experiment for the C. albicans CAF2-1 strain grown in YPD medium for 3 selected cells: cell 1, 3 and 4 (A) Total displacements (pixels) as a function of time for cell 1. (B) Distribution of the displacement/frame as a function of time for cell 1. (C) X-y displacement at the time point 0 min for cell 1. (D) X-y displacement at the time point 120 min for cell 1. (E) Total displacements (pixels) as a function of time for cell 3. (F) Distribution of the displacement/frame as a function of time for cell 3. (G) X-y displacement at the time point 0 min for cell 3. (H) X-y displacement at the time point 120 min for cell 3. (I) Total displacements (pixels) as a function of time for cell 4. (J) Distribution of the displacement/frame as a function of time for cell 4. (K) X-y displacement at the time point 0 min for cell 4. (L) X-y displacement at the time point 120 min for cell 4. Figure S5. Effect of the antifungal caspofungin (0.5 μg/mL) on the cellular nanomotion for 3 selected cells: cell 1, 10, and 12 of C. albicans CAF2-1. (A) Total displacements (pixels) as a function of time for cell 1. (B) Distribution of the displacement/frame as a function of time for cell 1. (C) X-y displacement at the time point 0 min for cell 1. (D) X-y displacement at the time point 300 min for cell 1. (E) Total displacements (pixels) as a function of time for cell 10. (F) Distribution of the displacement/frame as a function of time for cell 10. (G) X-y displacement at the time point 0 min for cell 10. (H) X-y displacement at the time point 300 min for cell 10. (I) Total displacements (pixels) as a function of time for cell 12. (J) Distribution of the displacement/frame as a function of time for cell 12. (K) X-y displacement at the time point 0 min for cell 12. (L) X-y displacement at the time point 300 min for cell 12. Figure S6. Effect of the antifungal caspofungin (1 μg/mL) on the cellular nanomotion for 2 selected cells: cell 1 and 2 of C. albicans CAF2-1. (A) Total displacements (pixels) as a function of time for cell 1. (B) Distribution of the displacement/frame as a function of time for cell 1. (C) X-y displacement at the time point 0 min for cell 1. (D) X-y displacement at the time point 300 min for cell 1. (E) Total displacements (pixels) as a function of time for cell 2. (F) Distribution of the displacement/frame as a function of time for cell 2. (G) X-y displacement at the time point 0 min for cell 2. (H) X-y displacement at the time point 300 min for cell 2. Figure S7. Effect of the antifungal caspofungin (100 μg/mL) on the cellular nanomotion for 3 selected cells: cell 5, 10 and 12 of C. albicans CAF2-1. (A) Total displacements (pixels) as a function of time for cell 5. (B) Distribution of the displacement/frame as a function of time for cell 5. (C) X-y displacement at the time point 0 min for cell 5. (D) X-y displacement at the time point 300 min for cell 5. (E) Total displacements (pixels) as a function of time for cell 10. (F) Distribution of the displacement/frame as a function of time for cell 10. (G) X-y displacement at the time point 0 min for cell 10. (H) X-y displacement at the time point 300 min for cell 10. (I) Total displacements (pixels) as a function of time for cell 12. (J) Distribution of the displacement/frame as a function of time for cell 12. (K) X-y displacement at the time point 0 min for cell 12. (L) X-y displacement at the time point 300 min for cell 12. Figure S8. Averaged cellular nanomotion for 20 cells of C. albicans CAF2-1. (A) Distribution of the displacements/frames during 2 h growth (control). (B) Distribution of the displacements/frames during 0.5 μg/mL fluconazole treatment. (C) Distribution of the displacements/frames during 1 μg/mL fluconazole treatment. (D) Distribution of the displacements/frames during 100 μg/mL fluconazole treatment. Figure S8. Averaged cellular nanomotion for 20 cells of C. albicans CAF2-1. (A) Distribution of the displacements/frames during 2 h growth (control). (B) Distribution of the displacements/frames during 0.5 μg/mL fluconazole treatment. (C) Distribution of the displacements/frames during 1 μg/mL fluconazole treatment. (D) Distribution of the displacements/frames during 100 μg/mL fluconazole treatment. Figure S10.

Effect of the antifungal fluconazole (1 μg/mL) on the cellular nanomotion for 2 selected cells: cell 18, and 19 of C. albicans CAF2-1. (A) Total displacements (pixels) as a function of time for cell 18. (B) Distribution of the displacement/frame as a function of time for cell 18. (C) X-y displacement at the time point 0 min for cell 18. (D) X-y displacement at the time point 300 min for cell 18. (E) Total displacements (pixels) as a function of time for cell 19. (F) Distribution of the displacement/frame as a function of time for cell 19. (G) X-y displacement at the time point 0 min for cell 19. (H) X-y displacement at the time point 300 min for cell 19. Figure S11. Effect of the antifungal fluconazole (100 μg/mL) on the cellular nanomotion for 3 selected cells: cell 2, 3, and 4 of C. albicans CAF2-1. (A) Total displacements (pixels) as a function of time for cell 2. (B) Distribution of the displacement/frame as a function of time for cell 2. (C) X-y displacement at the time point 0 min for cell 2. (D) X-y displacement at the time point 300 min for cell 2. (E) Total displacements (pixels) as a function of time for cell 3. (F) Distribution of the displacement/frame as a function of time for cell 3. (G) X-y displacement at the time point 0 min for cell 3. (H) X-y displacement at the time point 300 min for cell 3. (I) Total displacements (pixels) as a function of time for cell 4. (J) Distribution of the displacement/frame as a function of time for cell 4. (K) X-y displacement at the time point 0 min for cell 4. (L) X-y displacement at the time point 300 min for cell 4. Figure S12. Control experiment for the C. albicans DSY1024 strain grown in YPD medium for 3 selected cells: cell 1, 5 and 10. (A) Total displacements (pixels) as a function of time for cell 1. (B) Distribution of the displacement/frame as a function of time for cell 1. (C) X-y displacement at the time point 0 min for cell 1. (D) X-y displacement at the time point 120 min for cell 1. (E) Total displacements (pixels) as a function of time for cell 5. (F) Distribution of the displacement/frame as a function of time for cell 5. (G) X-y displacement at the time point 0 min for cell 5. (H) X-y displacement at the time point 120 min for cell 5. (I) Total displacements (pixels) as a function of time for cell 10. (J) Distribution of the displacement/frame as a function of time for cell 10. (K) X-y displacement at the time point 0 min for cell 10. (L) X-y displacement at the time point 120 min for cell 10. Figure S13. Averaged cellular nanomotion for 20 cells of C. albicans DSY1024. (A) Distribution of the displacements/frames during 2 h growth (control). (B) Distribution of the displacements/frames during 0.5 μg/mL fluconazole treatment. (C) Distribution of the displacements/frames during 1 μg/mL fluconazole treatment. (D) Distribution of the displacements/frames during 100 μg/mL fluconazole treatment. Figure S14. Effect of the antifungal fluconazole (0.5 μg/mL) on the cellular nanomotion for 3 selected cells: cell 2, 3 and 4 of C. albicans DSY1024. (A) Total displacements (pixels) as a function of time for cell 2. (B) Distribution of the displacement/frame as a function of time for cell 2. (C) X-y displacement at the time point 0 min for cell 2. (D) X-y displacement at the time point 300 min for cell 2. (E) Total displacements (pixels) as a function of time for cell 3. (F) Distribution of the displacement/frame as a function of time for cell 3. (G) X-y displacement at the time point 0 min for cell 3. (H) X-y displacement at the time point 300 min for cell 3. (I) Total displacements (pixels) as a function of time for cell 4. (J) Distribution of the displacement/frame as a function of time for cell 4. (K) X-y displacement at the time point 0 min for cell 4. (L) X-y displacement at the time point 300 min for cell 4. Figure S15. Effect of the antifungal fluconazole (1 μg/mL) on the cellular nanomotion for 2 selected cells: cell 2 and 5 of C. albicans DSY1024. (A) Total displacements (pixels) as a function of time for cell 2. (B) Distribution of the displacement/frame as a function of time for cell 2. (C) X-y displacement at the time point 0 min for cell 2. (D) X-y displacement at the time point 300 min for cell 2. (E) Total displacements (pixels) as a function of time for cell 5. (F) Distribution of the displacement/frame as a function of time for cell 5. (G) X-y displacement at the time point 0 min for cell 5. (H) X-y displacement at the time point 300 min for cell 5. Figure S16. Effect of the antifungal fluconazole (100 μg/mL) on the cellular nanomotion for 3 selected cells: cell 1, 2, and 3 of C. albicans DSY1024. (A) Total displacements (pixels) as a function of time for cell 1. (B) Distribution of the displacement/frame as a function of time for cell 1. (C) X-y displacement at the time point 0 min for cell 1. (D) X-y displacement at the time point 300 min for cell 1. (E) Total displacements (pixels) as a function of time for cell 2. (F) Distribution of the displacement/frame as a function of time for cell 2. (G) X-y displacement at the time point 0 min for cell 2. (H) X-y displacement at the time point 300 min for cell 2. (I) Total displacements (pixels) as a function of time for cell 3. (J) Distribution of the displacement/frame as a function of time for cell 3. (K) X-y displacement at the time point 0 min for cell 3. (L) X-y displacement at the time point 300 min for cell 3. Figure S17. Averaged cellular nanomotion for 20 cells of C. albicans DSY1024. (A) Distribution of the displacements/frames during 2 h growth (control). (B) Distribution of the displacements/frames during 0.5 μg/mL caspofungin treatment. (C) Distribution of the displacements/frames during 1 μg/mL caspofungin treatment. (D) Distribu-

tion of the displacements/frames during 100 μg/mL caspofungin treatment. Figure S18. Effect of the antifungal caspofungin (0.5 μg/mL) on the cellular nanomotion for 3 selected cells: cell 3, 12 and 14 of C. albicans DSY1024. (A) Total displacements (pixels) as a function of time for cell 3. (B) Distribution of the displacement/frame as a function of time for cell 3. (C) X-y displacement at the time point 0 min for cell 3. (D) X-y displacement at the time point 300 min for cell 3. (E) Total displacements (pixels) as a function of time for cell 12. (F) Distribution of the displacement/frame as a function of time for cell 12. (G) X-y displacement at the time point 0 min for cell 12. (H) X-y displacement at the time point 300 min for cell 12. (I) Total displacements (pixels) as a function of time for cell 14. (J) Distribution of the displacement/frame as a function of time for cell 14. (K) X-y displacement at the time point 0 min for cell 14. (L) X-y displacement at the time point 300 min for cell 14. Figure S19. Effect of the antifungal caspofungin (1 μg/mL) on the cellular nanomotion for 2 selected cells: cell 9 and 13 of C. albicans DSY1024. (A) Total displacements (pixels) as a function of time for cell 9. (B) Distribution of the displacement/frame as a function of time for cell 9. (C) X-y displacement at the time point 0 min for cell 9. (D) X-y displacement at the time point 300 min for cell 9. (E) Total displacements (pixels) as a function of time for cell 13. (F) Distribution of the displacement/frame as a function of time for cell 13. (G) X-y displacement at the time point 0 min for cell 13. (H) X-y displacement at the time point 300 min for cell 13. Figure S20. Effect of the antifungal caspofungin (100 μg/mL) on the cellular nanomotion for 3 selected cells: cell 2, 6, and 19 of C. albicans DSY1024. (A) Total displacements (pixels) as a function of time for cell 2. (B) Distribution of the displacement/frame as a function of time for cell 2. (C) X-y displacement at the time point 0 min for cell 2. (D) X-y displacement at the time point 300 min for cell 2. (E) Total displacements (pixels) as a function of time for cell 6. (F) Distribution of the displacement/frame as a function of time for cell 6. (G) X-y displacement at the time point 0 min for cell 6. (H) X-y displacement at the time point 300 min for cell 6. (I) Total displacements (pixels) as a function of time for cell 19. (J) Distribution of the displacement/frame as a function of time for cell 19. (K) X-y displacement at the time point 0 min for cell 19. (L) X-y displacement at the time point 300 min for cell 19. Figure S21. The slopes of the decrease in the total displacement of 20 cells as a function of time are calculated based on the time points 10, 60, 120, 180, 240, and 300 min during 1 μg/mL caspofungin or fluconazole treatment of the C. albicans strains: (A) caspofungin treated CAF2-1, (B) fluconazole treated CAF2-1, (C) caspofungin treated DSY1024, (D) fluconazole treated DSY1024; and during the 2 h growth in YDP medium (E) CAF2-1 and (F) DSY1024. Figure S22. The slopes of the decrease in the total displacement as a function of time are calculated based on the time points 10, 60, 120, 180, 240, and 300 min during 1 μg/mL caspofungin or fluconazole treatment for the averages of total displacements of all 20 cells: (A) caspofungin treated CAF2-1, (B) caspofungin treated DSY1024, (C) fluconazole treated CAF2-1, (D) fluconazole treated DSY1024; and during the 2 h growth in YDP medium of (E) CAF2-1 and (F) DSY1024. Figure S23. Comparison of the nanomotion of 20 living C. albicans CAF2-1 cells to 20 dead cell. (A) Total displacement of 20 cells of untreated living cells (time = o min) and 70 % (v/v) ethanol killed cells after 1 h of treatment; Wilcoxon test: **** $p < 0.0001$. (B) Image of PI stained dead cells in the microwells (after 1 h treatment with 70% (v/v) ethanol). (C) Total displacement of 20 single living cells (time = 0 min). (D) Total displacement of 20 single dead cells (time = 60 min). Figure S24. Comparison of the averaged cellular nanomotion for 20 cells of the C. albicans azole hypersusceptible DSY1024 strain treated with fluconazole (green) or caspofungin (blue) at a concentration of (A) 0.1 μg/mL, (B) 0.5 μg/mL, and (C) 100 μg/mL.

Author Contributions: Conceptualisation, R.G.W. and S.K.; methodology, R.G.W., V.R., C.Y., M.I.V., and S.K.; software, S.K. and M.I.V.; validation, V.R., C.Y., and R.G.W.; formal analysis, V.R.; resources, R.G.W. and S.K.; data curation, V.R.; writing—original draft preparation, R.G.W., V.R., C.Y., M.I.V., and S.K.; writing—review and editing, R.G.W., V.R., C.Y., M.I.V., B.D., and S.K.; visualisation, V.R. and R.G.W.; supervision, R.G.W., S.K., and B.D.; project administration, R.G.W. and S.K.; funding acquisition, R.G.W., S.K., and B.D. All authors have read and agreed to the published version of the manuscript.

Funding: This research was funded by the Belgian Federal Science Policy Office (Belspo) and the European Space Agency (ESA), grant number PRODEX Flumias Nanomotion; FWO, grant number I002620; FWO-SNSF, grant number 310030L_197946; FWO-SB-FDW Ph.D. grant of VR. IV and SK were supported by SNSF grants CRSII5_173863.

Institutional Review Board Statement: Not applicable.

Informed Consent Statement: Not applicable.

Data Availability Statement: All data needed to evaluate the conclusions in the paper are present in the paper and/or the Supplementary Materials. Additional data related to this paper may be requested from the authors.

Acknowledgments: The Research Council of the Vrije Universiteit Brussel (Belgium) and the University of Ghent (Belgium) are acknowledged for their support to the Alliance Research Group VUB-UGhent NanoMicrobiology (NAMI), and the International Joint Research Group (IJRG) VUBEPFL BioNanotechnology and NanoMedicine (NANO).

Conflicts of Interest: The authors declare no conflict of interest.

References

1. Lopes, J.P.; Lionakis, M.S. Pathogenesis and virulence of *Candida albicans*. *Virulence* **2021**, *13*, 89–121. [CrossRef]
2. Dadar, M.; Tiwari, R.; Karthik, K.; Chakraborty, S.; Shahali, Y.; Dhama, K. Candida albicans—Biology, molecular characterization, pathogenicity, and advances in diagnosis and control—An update. *Microb. Pathog.* **2018**, *117*, 128–138. [CrossRef]
3. Poulain, D. Candida albicans, plasticity and pathogenesis. *Crit. Rev. Microbiol.* **2015**, *41*, 208–217. [CrossRef] [PubMed]
4. Pilmis, B.; Yang, Z.; Lanternier, F.; Lortholary, O. Systemic Candidiasis. In *Infectious Diseases*; Elsevier: Amsterdam, The Netherlands, 2017; pp. 439–445.e1. [CrossRef]
5. Durand, C.; Maubon, D.; Cornet, M.; Wang, Y.; Aldebert, D.; Garnaud, C. Can We Improve Antifungal Susceptibility Testing? *Front. Cell. Infect. Microbiol.* **2021**, *11*, 720609. [CrossRef]
6. Knabl, L.; Lass-Flörl, C. Antifungal susceptibility testing in *Candida* species: Current methods and promising new tools for shortening the turnaround time. *Expert Rev. Anti-infective Ther.* **2020**, *18*, 779–787. [CrossRef]
7. CLSI. *Reference Method for Broth Dilution Antifungal Susceptibility Testing of Filamentous Fungi*; Approved Standard—2nd ed. CLSI document M38-A2; Clinical and Laboratory Standards Institute: Wayne, PA, USA, 2008.
8. Van Belkum, A.; Burnham, C.-A.D.; Rossen, J.W.A.; Mallard, F.; Rochas, O.; Dunne, W.M., Jr. Innovative and rapid antimicrobial susceptibility testing systems. *Nat. Rev. Microbiol.* **2020**, *18*, 1–13. [CrossRef] [PubMed]
9. Posteraro, B.; Torelli, R.; De Carolis, E.; Posteraro, P.; Sanguinetti, M. Antifungal susceptibility testing: Current role from the clinical laboratory perspective. *Mediterr. J. Hematol. Infect. Dis.* **2014**, *6*, e2014030. [CrossRef]
10. Pfaller, M.A. Antifungal Drug Resistance: Mechanisms, Epidemiology, and Consequences for Treatment. *Am. J. Med.* **2012**, *125*, S3–S13. [CrossRef] [PubMed]
11. Hayden, R.T.; Clinton, L.K.; Hewitt, C.; Koyamatsu, T.; Sun, Y.; Jamison, G.; Perkins, R.; Tang, L.; Pounds, S.; Bankowski, M.J. Rapid Antimicrobial Susceptibility Testing Using Forward Laser Light Scatter Technology. *J. Clin. Microbiol.* **2016**, *54*, 2701–2706. [CrossRef]
12. Johnson, W.L.; France, D.C.; Rentz, N.S.; Cordell, W.T.; Walls, F.L. Sensing bacterial vibrations and early response to antibiotics with phase noise of a resonant crystal. *Sci. Rep.* **2017**, *7*, 12138. [CrossRef]
13. Cowger, T.A.; Yang, Y.; Rink, D.E.; Todd, T.; Chen, H.; Shen, Y.; Yan, Y.; Xie, J. Protein-Adsorbed Magnetic-Nanoparticle-Mediated Assay for Rapid Detection of Bacterial Antibiotic Resistance. *Bioconjugate Chem.* **2017**, *28*, 890–896. [CrossRef] [PubMed]
14. Shi, X.; Kadiyala, U.; VanEpps, J.S.; Yau, S.-T. Culture-free bacterial detection and identification from blood with rapid, phenotypic, antibiotic susceptibility testing. *Sci. Rep.* **2018**, *8*, 3416. [CrossRef] [PubMed]
15. Kittel, M.; Findeisen, P.; Ghebremedhin, B.; Miethke, T.; Grundt, A.; Ahmad-Nejad, P.; Neumaier, M. Rapid susceptibility testing of multi-drug resistant *Escherichia coli* and *Klebsiella* by glucose metabolization monitoring. *Clin. Chem. Lab. Med.* **2019**, *57*, 1271–1279. [CrossRef] [PubMed]
16. Chung, C.-Y.; Wang, J.-C.; Chuang, H.-S. Rapid Bead-Based Antimicrobial Susceptibility Testing by Optical Diffusometry. *PLoS ONE* **2016**, *11*, e0148864. [CrossRef] [PubMed]
17. Iriya, R.; Syal, K.; Jing, W.; Mo, M.; Yu, H.; Haydel, S.E.; Wang, S.; Tao, N. Real-time detection of antibiotic activity by measuring nanometer-scale bacterial deformation. *J. Biomed. Opt.* **2017**, *22*, 126002–126009. [CrossRef] [PubMed]
18. Sparbier, K.; Schubert, S.; Kostrzewa, M. MBT-ASTRA: A suitable tool for fast antibiotic susceptibility testing? *Methods* **2016**, *104*, 48–54. [CrossRef] [PubMed]
19. Ibarlucea, B.; Rim, T.; Baek, C.K.; de Visser, J.A.G.M.; Baraban, L.; Cuniberti, G. Nanowire sensors monitor bacterial growth kinetics and response to antibiotics. *Lab Chip* **2017**, *17*, 4283–4293. [CrossRef] [PubMed]
20. Kuss, S.; Couto, R.A.D.S.; Evans, R.M.; Lavender, H.; Tang, C.C.; Compton, R.G. Versatile Electrochemical Sensing Platform for Bacteria. *Anal. Chem.* **2019**, *91*, 4317–4322. [CrossRef] [PubMed]
21. Idelevich, E.A.; Hoy, M.; Görlich, D.; Knaack, D.; Grünastel, B.; Peters, G.; Borowski, M.; Becker, K. Rapid Phenotypic Detection of Microbial Resistance in Gram-Positive Bacteria by a Real-Time Laser Scattering Method. *Front. Microbiol.* **2017**, *8*, 1064. [CrossRef]
22. e Silva, D.F.; Silva-Dias, A.; Gomes, R.; Martins-Oliveira, I.; Ramos, M.; Rodrigues, A.; Cantón, R.; Pina-Vaz, C. Evaluation of rapid colistin susceptibility directly from positive blood cultures using a flow cytometry assay. *Int. J. Antimicrob. Agents* **2019**, *54*, 820–823. [CrossRef]
23. Tannert, A.; Grohs, R.; Popp, J.; Neugebauer, U. Phenotypic antibiotic susceptibility testing of pathogenic bacteria using photonic readout methods: Recent achievements and impact. *Appl. Microbiol. Biotechnol.* **2018**, *103*, 549–566. [CrossRef] [PubMed]

24. Gao, J.; Li, H.; Torab, P.; Mach, K.E.; Craft, D.W.; Thomas, N.J.; Puleo, C.M.; Liao, J.C.; Wang, T.-H.; Wong, P.K. Nanotube assisted microwave electroporation for single cell pathogen identification and antimicrobial susceptibility testing. *Nanomed. Nanotechnol. Biol. Med.* **2019**, *17*, 246–253. [CrossRef]
25. Novelli-Rousseau, A.; Espagnon, I.; Filiputti, D.; Gal, O.; Douet, A.; Mallard, F.; Josso, Q. Culture-free Antibiotic-susceptibility Determination from Single-bacterium Raman Spectra. *Sci. Rep.* **2018**, *8*, 3957. [CrossRef] [PubMed]
26. Pitruzzello, G.; Thorpe, S.; Johnson, S.; Evans, A.; Gadêlha, H.; Krauss, T.F. Multiparameter antibiotic resistance detection based on hydrodynamic trapping of individual *E. coli*. *Lab Chip* **2019**, *19*, 1417–1426. [CrossRef] [PubMed]
27. Yu, H.; Jing, W.; Iriya, R.; Yang, Y.; Syal, K.; Mo, M.; Grys, T.E.; Haydel, S.E.; Wang, S.; Tao, N. Phenotypic Antimicrobial Susceptibility Testing with Deep Learning Video Microscopy. *Anal. Chem.* **2018**, *90*, 6314–6322. [CrossRef]
28. Correa-Martínez, C.L.; Idelevich, E.A.; Sparbier, K.; Kostrzewa, M.; Becker, K. Rapid Detection of Extended-Spectrum β-Lactamases (ESBL) and AmpC β-Lactamases in Enterobacterales: Development of a Screening Panel Using the MALDI-TOF MS-Based Direct-on-Target Microdroplet Growth Assay. *Front. Microbiol.* **2019**, *10*, 13. [CrossRef] [PubMed]
29. Köck, R.; Wüllenweber, J.; Horn, D.; Lanckohr, C.; Becker, K.; Idelevich, E.A. Implementation of short incubation MALDI-TOF MS identification from positive blood cultures in routine diagnostics and effects on empiric antimicrobial therapy. *Antimicrob. Resist. Infect. Control.* **2017**, *6*, 12. [CrossRef]
30. Kohler, A.; Venturelli, L.; Longo, G.; Dietler, G.; Kasas, S. Nanomotion detection based on atomic force microscopy cantilevers. *Cell Surf.* **2019**, *5*, 100021. [CrossRef]
31. Longo, G.; Alonso-Sarduy, L.; Rio, L.M.; Bizzini, A.; Trampuz, A.; Notz, J.; Dietler, G.; Kasas, S. Rapid detection of bacterial resistance to antibiotics using AFM cantilevers as nanomechanical sensors. *Nat. Nanotechnol.* **2013**, *8*, 522–526. [CrossRef]
32. Kasas, S.; Ruggeri, F.S.; Benadiba, C.; Maillard, C.; Stupar, P.; Tournu, H.; Dietler, G.; Longo, G. Detecting nanoscale vibrations as signature of life. *Proc. Natl. Acad. Sci. USA* **2014**, *112*, 378–381. [CrossRef]
33. Villalba, M.I.; Stupar, P.; Chomicki, W.; Bertacchi, M.; Dietler, G.; Arnal, L.; Vela, M.E.; Yantorno, O.; Kasas, S. Nanomotion Detection Method for Testing Antibiotic Resistance and Susceptibility of Slow-Growing Bacteria. *Small* **2017**, *14*. [CrossRef]
34. Venturelli, L.; Kohler, A.; Stupar, P.; Villalba, M.I.; Kalauzi, A.; Radotic, K.; Bertacchi, M.; Dinarelli, S.; Girasole, M.; Pešić, M.; et al. A perspective view on the nanomotion detection of living organisms and its features. *J. Mol. Recognit.* **2020**, *33*, e2849. [CrossRef]
35. Kasas, S.; Malovichko, A.; Villalba, M.; Vela, M.; Yantorno, O.; Willaert, R. Nanomotion Detection-Based Rapid Antibiotic Susceptibility Testing. *Antibiotics* **2021**, *10*, 287. [CrossRef]
36. Syal, K.; Iriya, R.; Yang, Y.; Yu, H.; Wang, S.; Haydel, S.E.; Chen, H.-Y.; Tao, N. Antimicrobial Susceptibility Test with Plasmonic Imaging and Tracking of Single Bacterial Motions on Nanometer Scale. *ACS Nano* **2015**, *10*, 845–852. [CrossRef] [PubMed]
37. Syal, K.; Shen, S.; Yang, Y.; Wang, S.; Haydel, S.E.; Tao, N. Rapid Antibiotic Susceptibility Testing of Uropathogenic *E. coli* by Tracking Submicron Scale Motion of Single Bacterial Cells. *ACS Sens.* **2017**, *2*, 1231–1239. [CrossRef] [PubMed]
38. Bermingham, C.R.; Murillo, I.; Payot, A.D.; Balram, K.C.; Kloucek, M.B.; Hanna, S.; Antognozzi, M. Imaging of sub-cellular fluctuations provides a rapid way to observe bacterial viability and response to antibiotics. *bioRxiv* **2018**, 460139. [CrossRef]
39. Leonard, H.; Halachmi, S.; Ben-Dov, N.; Nativ, O.; Segal, E. Unraveling Antimicrobial Susceptibility of Bacterial Networks on Micropillar Architectures Using Intrinsic Phase-Shift Spectroscopy. *ACS Nano* **2017**, *11*, 6167–6177. [CrossRef] [PubMed]
40. Willaert, R.G.; Boer, P.V.; Malovichko, A.; Alioscha-Perez, M.; Radotić, K.; Bartolić, D.; Kalauzi, A.; Villalba, M.I.; Sanglard, D.; Dietler, G.; et al. Single yeast cell nanomotions correlate with cellular activity. *Sci. Adv.* **2020**, *6*, eaba3139. [CrossRef] [PubMed]
41. Radonicic, V.; Yvanoff, C.; Villalba, M.I.; Kasas, S.; Willaert, R.G. The Dynamics of Single-Cell Nanomotion Behaviour of *Saccharomyces cerevisiae* in a Microfluidic Chip for Rapid Antifungal Susceptibility Testing. *Fermentation* **2022**, *8*, 195. [CrossRef]
42. Marchetti, O.; Majcherczyk, P.A.; Glauser, M.P.; Bille, J.; Moreillon, P.; Sanglard, D. Sensitive Bioassay for Determination of Fluconazole Concentrations in Plasma Using a Candida albicans Mutant Hypersusceptible to Azoles. *Antimicrob. Agents Chemother.* **2001**, *45*, 696–700. [CrossRef]
43. A Fonzi, W.; Irwin, M.Y. Isogenic strain construction and gene mapping in Candida albicans. *Genetics* **1993**, *134*, 717–728. [CrossRef]
44. Davis, R.H.; Hunt, T.P. Modeling and Measurement of Yeast Flocculation. *Biotechnol. Prog.* **1986**, *2*, 91–97. [CrossRef]
45. Fontana, A.; Bore, C.; Ghommidh, C.; Guiraud, J.P. Structure and Sucrose Hydrolysis Activity of Saccharorn yces cerevisiae Aggregates. *Biotechnol. Bioeng.* **1992**, *40*, 475–482. [CrossRef]
46. van Hamersveld, E.H.; van der Lans, R.G.J.M.; Luyben, K.C.A.M. *Quantification of Brewers' Yeast Flocculation in a Stirred Tank: Effect of Physical Parameters on Flocculation*; John Wiley & Sons, Inc.: Hoboken, NJ, USA, 1997.
47. Haddad, S.A.; Lindegren, C.C. A Method for Determining the Weight of an Individual Yeast Cell. *Appl. Environ. Microbiol.* **1953**, *1*, 153–156. [CrossRef] [PubMed]
48. Guizar-Sicairos, M.; Thurman, S.T.; Fienup, J.R. Efficient subpixel image registration algorithms. *Opt. Lett.* **2008**, *33*, 156–158. [CrossRef] [PubMed]
49. Kwolek-Mirek, M.; Zadrag-Tecza, R. Comparison of methods used for assessing the viability and vitality of yeast cells. *FEMS Yeast Res.* **2014**, *14*, 1068–1079. [CrossRef]
50. Suwunnakorn, S.; Wakabayashi, H.; Kordalewska, M.; Perlin, D.S.; Rustchenko, E. *FKS2* and *FKS3* Genes of Opportunistic Human Pathogen Candida albicans Influence Echinocandin Susceptibility. *Antimicrob. Agents Chemother.* **2018**, *62*, e02299-17. [CrossRef]
51. Sanglard, D.; Ischer, F.; Marchetti, O.; Entenza, J.; Bille, J. Calcineurin A of Candida albicans: Involvement in antifungal tolerance, cell morphogenesis and virulence. *Mol. Microbiol.* **2003**, *48*, 959–976. [CrossRef]

52. Cordeiro, R.A.; Teixeira, C.E.C.; Brilhante, R.S.N.; Castelo-Branco, D.S.C.M.; Paiva, M.A.N.; Leite, J.J.G.; Lima, D.T.; Monteiro, A.J.; Sidrim, J.J.C.; Rocha, M.F.G. Minimum inhibitory concentrations of amphotericin B, azoles and caspofungin against *Candida* species are reduced by farnesol. *Med. Mycol.* **2013**, *51*, 53–59. [CrossRef] [PubMed]
53. Marchetti, O.; Moreillon, P.; Entenza, J.M.; Vouillamoz, J.; Glauser, M.P.; Bille, J.; Sanglard, D. Fungicidal Synergism of Fluconazole and Cyclosporine in *Candida albicans* Is Not Dependent on Multidrug Efflux Transporters Encoded by the *CDR1*, *CDR2*, *CaMDR1*, and *FLU1* Genes. *Antimicrob. Agents Chemother.* **2003**, *47*, 1565–1570. [CrossRef] [PubMed]
54. Rettig, J.R.; Folch, A. Large-Scale Single-Cell Trapping and Imaging Using Microwell Arrays. *Anal. Chem.* **2005**, *77*, 5628–5634. [CrossRef] [PubMed]
55. Hoang, A. Caspofungin acetate: An antifungal agent. *Am. J. Health Pharm.* **2001**, *58*, 1206–1214. [CrossRef] [PubMed]
56. Lu, H.; Shrivastava, M.; Whiteway, M.; Jiang, Y. *Candida albicans* targets that potentially synergize with fluconazole. *Crit. Rev. Microbiol.* **2021**, *47*, 323–337. [CrossRef] [PubMed]
57. Pristov, K.E.; Ghannoum, M.A. Resistance of Candida to azoles and echinocandins worldwide. *Clin. Microbiol. Infect.* **2019**, *25*, 792–798. [CrossRef] [PubMed]
58. Berman, J.; Krysan, D.J. Drug resistance and tolerance in fungi. *Nat. Rev. Genet.* **2020**, *18*, 319–331. [CrossRef]
59. Willaert, R.G. Micro- and Nanoscale Approaches in Antifungal Drug Discovery. *Fermentation* **2018**, *4*, 43. [CrossRef]
60. Morschhäuser, J. The genetic basis of fluconazole resistance development in Candida albicans. *Biochim. Biophys. Acta Mol. Basis Dis.* **2002**, *1587*, 240–248. [CrossRef]
61. Pourakbari, B.; Teymuri, M.; Mahmoudi, S.; Valian, S.K.; Movahedi, Z.; Eshaghi, H.; Mamishi, S. Expression of Major Efflux Pumps in Fluconazole-Resistant Candida albicans. *Infect. Disord. Drug Targets* **2017**, *17*, 178–184. [CrossRef]
62. Calabrese, D.; Bille, J.; Sanglard, D. A novel multidrug efflux transporter gene of the major facilitator superfamily from Candida albicans (FLU1) conferring resistance to fluconazole. *Microbiology* **2000**, *146*, 2743–2754. [CrossRef]
63. Villalba, M.I.; Rossetti, E.; Bonvallat, A.; Yvanoff, C.; Radonicic, V. Simple optical nanomotion method for single-bacterium viability and antibiotic response testing. *Proc. Natl. Acad. Sci. USA* **2023**.
64. Roslon, I.; Japaridze, A.; Rodenhuis, S.; Hamoen, L.; Ghatkesar, M.; Steeneken, P.; Alijani, F. Microwell-enhanced optical detection of single bacteria. *bioRxiv* **2023**. [CrossRef]
65. Rosłoń, I.E.; Japaridze, A.; Steeneken, P.G.; Dekker, C.; Alijani, F. Probing nanomotion of single bacteria with graphene drums. *Nat. Nanotechnol.* **2022**, *17*, 637–642. [CrossRef] [PubMed]
66. Starodubtseva, M.N.; Chelnokova, I.A.; Shkliarava, N.M.; Villalba, M.I.; Tapalski, D.V.; Kasas, S.; Willaert, R.G. Modulation of the nanoscale motion rate of Candida albicans by X-rays. *Front. Microbiol.* **2023**, *14*, 833. [CrossRef]